

**DESIGN OF ZEONEX BASED POLARIZATION  
MAINTAINING LOW LOSS POROUS CORE FIBER FOR  
TERAHERTZ REGIME**

By

Md. Anwar Sadath

**A thesis submitted to the Department of Electrical and Electronic Engineering of  
Bangladesh University of Engineering and Technology in partial fulfillment of the  
requirement for the degree of**

**MASTER OF SCIENCE IN ELECTRICAL AND ELECTRONIC  
ENGINEERING**

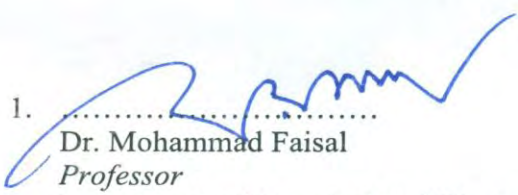


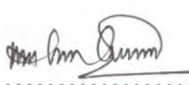


Department of Electrical and Electronic Engineering  
BANGLADESH UNIVERSITY OF ENGINEERING AND  
TECHNOLOGY

January 2019

The thesis titled “**DESIGN OF ZEONEX BASED POLARIZATION MAINTAINING LOW LOSS POROUS CORE FIBER FOR TERAHERTZ REGIME**” submitted by Md. Anwar Sadath, Roll No.: 0416062294, Session: April, 2016, has been accepted as satisfactory in partial fulfillment of the requirement for the degree of Master of Science in Electrical and Electronic Engineering on 16 January 2019.

## BOARD OF EXAMINERS

1.   
.....  
Dr. Mohammad Faisal  
*Professor*  
Department of Electrical and Electronic Engineering  
Bangladesh University of Engineering and Technology (BUET)  
Dhaka – 1205, Bangladesh  
Chairman  
(Supervisor)
2.   
.....  
Dr. Md. Shafiqul Islam  
*Professor and Head*  
Department of Electrical and Electronic Engineering  
Bangladesh University of Engineering and Technology (BUET)  
Dhaka – 1205, Bangladesh  
Member  
(Ex- officio)
3.   
.....  
Dr. Md. Shah Alam  
*Professor*  
Department of Electrical and Electronic Engineering  
Bangladesh University of Engineering and Technology (BUET)  
Dhaka – 1205, Bangladesh  
Member
4.   
.....  
Dr. S.M. Mostafa Al Mamun  
*Professor and Chairman*  
Department of Electrical and Electronic Engineering  
University of Dhaka (DU)  
Dhaka – 1205, Bangladesh  
Member  
(External)

## CANDIDATE'S DECLARATION

I, hereby declare that this is based on the results found by myself. Materials of work found by other researchers are mentioned by reference. This thesis, neither in whole nor in part, has been previously submitted for any degree.

Signature of the Candidate

.....

Md. Anwar Sadath

# **DEDICATION**

*TO MY DEAREST PARENTS AND GRAND-PARENTS*

## **ACKNOWLEDGMENT**

First and Foremost praise is to Almighty Allah, the greatest of all, on whom eventually we depend for sustenance and guidance. I would like to thank him for giving me opportunity, determination and strength to do my research. His continuous grace and mercy was with me throughout my life and ever more during the tenure of my research.

I would like to thank my supervisor Dr. Mohammad Faisal, Professor, Department of EEE, BUET, for the patient guidance, encouragement and advice he has provided me throughout my time as his student. I have been extremely lucky to have a supervisor who cared much about my work, and who responded my questions and quires so promptly. In addition to being an admirable supervisor, he is a man of principles and has immense knowledge of research in general and his subject in particular. I am deeply indebted to him for his steady guidance and inspiration in publishing my thesis technical papers in a renowned journal.

I would also like to thank the members of my thesis examination board, Dr. Md. Shafiqul Islam, Dr. Md. Shah Alam and Dr. S.M. Mostafa Al Mamun for their encouragement and insightful comments.

I am grateful to my colleagues who have helped and provided me adequate support for successful completion of research works. Most importantly, none of this would have been possible without the love and patience of my parents. I would like to express my heartfelt gratitude to my family.

## ABSTRACT

We present two novel Zeonex based single-mode ultra-high birefringent porous core micro-structured fibers, one consisting of slotted cladding with hybrid core and another consisting of elliptical shaped suspended core for THz wave guidance. Full-vector finite element method with perfectly matched layer boundary condition is used to investigate the wave guiding property including single mode operation, birefringence, effective material loss, confinement loss, core power fraction, dispersion, modal effective area and fiber nonlinearity of both fibers.

Addition of four circular air holes along with only three elliptical air holes in the core of the proposed model 1 enhances the value of birefringence to 0.0818 with an effective material loss of only  $0.0448 \text{ cm}^{-1}$  and a confinement loss of  $4 \times 10^{-7} \text{ cm}^{-1}$  at an operating frequency of 1 THz. Moreover, its compact slotted geometry in the cladding imposes as high as 55.3% of total modal power to flow through the core air holes. Furthermore, a near flattened dispersion of  $1.196 \pm 0.08 \text{ ps/THz/cm}$  for a broad frequency range (0.9-1.6THz) and fiber nonlinearity of  $3.33 \times 10^{-9} \text{ W}^{-1} \text{ m}^{-1}$  for an effective area of  $1.32 \times 10^5 \text{ } \mu\text{m}^2$  are obtained for x-polarized mode for the same operating frequency. On the other hand, model 2 at optimum design parameters shows an ultra high birefringence of 0.1116 which is the highest so far to the best of our knowledge, lower absorption loss of  $0.04716 \text{ cm}^{-1}$ , a negligible confinement loss of  $2.65 \times 10^{-7} \text{ cm}^{-1}$  and a low flat dispersion flattened characteristics over a wide terahertz band. Furthermore, the proposed model 2 allows a significant amount of total power to flow through the core air-slots. Moreover, due to its larger effective area, the proposed PCF demonstrates negligible non-linearity.

A latest cyclo-olefin polymer (COP) based material, trade name Zeonex, is chosen as the background material for both of our proposed model because of its unique advantages over other materials. Moreover, it has lower specific gravity, chemical resistance at elevated temperature, higher transparency, lower melt flow index etc. Furthermore, the physical properties of Zeonex are also suitable for high quality fiber drawing. Also, fluctuations in the fiber diameter are reduced because of the greater stability of drawing process. The proposed fibers can easily be fabricated using extrusion technology and would be suitable for polarization maintaining applications with a minimal absorption loss in the terahertz regime.

# TABLE OF CONTENTS

<b>ACKNOWLEDGMENT .....</b>	<b>ixi</b>
<b>ABSTRACT.....</b>	<b>v</b>
<b>LIST OF FIGURES .....</b>	<b>xiv</b>
<b>LIST OF TABLES .....</b>	<b>xvi</b>
<b>LIST OF ABBREVIATIONS .....</b>	<b>v</b>
<b>LIST OF SYMBOLS .....</b>	<b>xvi</b>
<b>1 INTRODUCTION.....</b>	<b>1</b>
1.1 Terahertz Radiation And Its Applications .....	1
1.2 Terahertz Waveguides .....	2
1.3 History of Photonic Crystal Fiber Based Terahertz Waveguides .....	2
1.4 Applications of PCF Based Terahertz Waveguides.....	4
1.5 Characterization of THz Waveguides.....	5
1.6 Classifications of THz waveguides.....	8
1.6.1 Metallic Waveguides .....	8
1.6.2 Dielectric Waveguides .....	8
1.7 Motivation of the Work .....	10
1.8 Objectives with specific aims and possible outcome.....	11
1.9 Organization of the thesis .....	11
<b>2 TERAHERTZ SOURCES AND DETECTORS.....</b>	<b>13</b>
2.1 Introduction.....	13
2.2 Terahertz Sources.....	13
2.2.1 Gas Lasers.....	14

2.2.2	Source derived from microwave technology .....	15
2.2.3	Free electron lasers and synchrotrons .....	15
2.2.4	Photoconductive Antenna .....	15
2.2.5	Parametric interaction in non-linear crystal .....	16
2.2.6	Optical rectifications in gases .....	17
2.2.7	Quantum cascade lasers .....	17
2.3	Terahertz Detectors.....	18
2.3.1	Photoconductive antenna .....	18
2.3.2	Electro-optic sampling.....	18
2.3.3	Bolometers .....	19
2.4	Conclusion .....	19
<b>3</b>	<b>TERAHERTZ WAVEGUIDE MATERIALS.....</b>	<b>20</b>
3.1	Introduction.....	20
3.2	Polymethylmethacrylate or PMMA .....	20
3.2.1	Advantages and disadvantages of PMMA .....	20
3.2.2	Properties of PMMA.....	21
3.3	High density polyethylene of HDPE.....	22
3.3.1	Advantages and disadvantages of HDPE.....	22
3.3.3	Properties of HDPE.....	23
3.4	Teflon.....	24
3.4.1	Advantages and disadvantages of teflon.....	24
3.4.3	Properties of teflon.....	25
3.5	Topas.....	25
3.5.1	Advantages and disadvantages of topas.....	26
3.5.3	Properties of topas.....	27
3.6	Zeonex .....	27
3.6.1	Advantages of Zeonex .....	27



3.6.2	Properties of zeonex.....	28
3.7	Conclusion .....	28
<b>4</b>	<b>THEORETICAL ANALYSIS OF THZ FIBERS .....</b>	<b>29</b>
4.1	Introduction.....	29
4.2	Wave Propagation.....	29
4.3	Finite Element Method .....	31
4.4	Characteristic Parameters.....	32
4.4.1	Effective Refractive Index .....	32
4.4.2	Normalized Frequency of $V$ -parameter.....	33
4.4.3	Effective Material Loss.....	33
4.4.4	Confinement Loss .....	34
4.4.5	Dispersion .....	34
4.4.6	Birefringence .....	34
4.4.7	Power Fraction .....	35
4.4.8	Effective area and non-linearity.....	35
4.5	Conclusion .....	36
<b>5</b>	<b>PROPOSED MODELS AND SIMULATION RESULTS .....</b>	<b>37</b>
5.1	Introduction.....	37
5.2	Proposed Models.....	37
5.3	Simulation Results .....	40
5.3.1	Simulation result of proposed model 1 .....	40
5.3.2	Simulation result of proposed model 2.....	53
5.4	Fabrication Possibilities .....	60
5.5	Conclusion .....	61

<b>6</b>	<b>CONCLUSION .....</b>	<b>62</b>
6.1	Introduction.....	62
6.2	Conclusion. ....	62
6.3	Future Work. ....	63

## LIST OF FIGURES

Figure 1.1:	Electromagnetic Frequency Spectrum.....	1
Figure 1.2:	Applications THz waves.....	2
Figure 1.3:	Schematic of the devices required for characterization of THz waveguides...	7
Figure 1.4:	Hollow core metallic waveguide.....	8
Figure 1.5:	Circular dielectric waveguide.....	9
Figure 2.1:	THz Sources.....	14
Figure 2.2:	Gas Laser.....	14
Figure 2.3:	Photoconductive Antenna as THz Source.....	16
Figure 2.4:	Quantum Cascade Laser.....	17
Figure 2.5:	Photoconductive Antenna as THz detector.....	18
Figure 5.1:	Cross Sectional view of the proposed model 1.....	38
Figure 5.2:	Cross Sectional view of the proposed model 2.....	39
Figure 5.3:	(a) Mesh of the proposed PCF (model 1); Mode field distribution at $L_c = 400\mu\text{m}$ and $f = 1\text{ THz}$ for (b) x-polarization mode; and (c) y-polarization mode.....	41
Figure 5.4:	Effective refractive index as a function of core length at $f=1\text{ THz}$ for model 1.....	41
Figure 5.5:	Effective refractive index as a function of frequency at $L_c = 400\mu\text{m}$ for model 1.....	42
Figure 5.6:	V-parameter as a function core length at $f = 1\text{ THz}$ for model 1.....	43
Figure 5.7:	V-parameter as a function of frequency at $L_c=400\mu\text{m}$ for model 1.....	43
Figure 5.8:	EML as a function of core length at $f = 1\text{ THz}$ for model 1.....	44
Figure 5.9:	EML as a function of frequency at $L_c = 400\mu\text{m}$ for model 1.....	45
Figure 5.10:	Birefringence as a function core length at $f=1\text{ THz}$ for model 1.....	46
Figure 5.11:	Birefringence as a function of frequency at $L_c = 400\mu\text{m}$ for model 1.....	46
Figure 5.12:	Group birefringence as a function of frequency at $L_c = 400\mu\text{m}$ for model 1.....	47

Figure 5.13: Dispersion as a function of frequency at $L_c = 400\mu\text{m}$ for model 1.....	48
Figure 5.14: Confinement loss as a function of core length at $f=1\text{THz}$ for model 1.....	48
Figure 5.15: Confinement loss as a function of frequency at $L_c=400\mu\text{m}$ for model 1.....	49
Figure 5.16: Core power fraction as a function of core length at $f = 1\text{ THz}$ for model 1.....	50
Figure 5.17: Core power fraction as a function of frequency at $L_c=400\mu\text{m}$ for model 1.....	50
Figure 5.18: Effective area of the fiber as a function of core length at $f=1\text{ THz}$ for model 1.....	52
Figure 5.19: Effective area of the fiber as a function of frequency at $L_c=400\mu\text{m}$ for model 1.....	52
Figure 5.20: Nonlinearity $\gamma$ of the fiber as a function of frequency at $L_c=400\mu\text{m}$ for model 1.....	52
Figure 5.21: Figure 5.20: Mode power distribution for model 2 (a) x-polarized mode (b) y-polarized mode.....	53
Figure 5.22: Effective refractive index as a function of frequency at $2a=440\mu\text{m}$ for model 2.....	54
Figure 5.23: Birefringence as a function of frequency at $2a=440\mu\text{m}$ for model 2.....	54
Figure 5.24: Group birefringence as a function of frequency at $2a = 440\mu\text{m}$ for model 2.....	55
Figure 5.25: EML as a function of frequency at $2a=400\mu\text{m}$ for model 2.....	56
Figure 5.26: Confinement loss as a function of frequency at $2a=440\mu\text{m}$ for model 2.....	56
Figure 5.27: Dispersion as a function of frequency at $2a=440\mu\text{m}$ for model 2.....	57
Figure 5.28: Air core power fraction as a function of frequency at $2a=440\mu\text{m}$ for model 2.....	58
Figure 5.29: Effective area of the fiber as a function of frequency at $2a=440\mu\text{m}$ for model 2.....	59
Figure5.30: Non-linearity of the fiber as a function of frequency at $2a=440\mu\text{m}$ for model 2.....	59

## LIST OF TABLES

Table 3-1: Properties of PMMA.....	21
Table 3-2: Properties of HDPE.....	23
Table 3-3: Properties of Teflon.....	24
Table 3-4: Properties of Topas.....	26
Table 3-5: Properties of Zeonex.....	27
Table 5-1: Comparison of different characteristics of the proposed PCF with some other PCF's.....	60

## LIST OF ABBREVIATIONS

<b>Symbol</b>	<b>Meaning</b>	<b>Section</b>
THz	Terahertz	1.1
OFs	Optical Fibers	1.3
PCFs	Photonic Crystal Fibers	1.3
PMMA	Polymethyl Methacrylate	1.3
HDPE	High density polyethylene	1.3
COP	Cyclo-Olefin Polymer	1.3
IR	Infrared Radiation	1.6.2
MOFs	Microstructured Optical Fibers	1.6.2
CO <sub>2</sub>	Carbon Dioxide	2.2.1
DC	Direct Current	2.2.4
MSM	Metal Semiconductor Metal	2.2.4
InSb	Indium Antimonide	2.2.3
PCA	Photoconductive Antenna	2.4
OR	Optical Rectification	2.4
MMA	Methyl Methacrylate	3.2
UV	Ultraviolet	3.2.1
MPa	Megapascal	3.2.3
GPa	Modulus of Elasticity	3.2.3
PEHD	Polyethylene High-Density	3.3
PTFE	Polytetrafluoroethylene	3.4

TFE	Tetra-Fluoro-Ethylene	3.4
COC	Cyclic Olefin Copolymers	3.5
MKS	Meter Kilogram Second	4.2
EML	Effective Material Loss	5.3.1
FEM	Finite Element modeling	5.3.2
PML	Perfectly Matched Layer	5.3.2
MTIR	Modified Total Internal Reflection	5.3.2
MMA	Methyl Methacrylate	5.4

## LIST OF SYMBOLS

Symbol	Meaning	Section
$T_g$	Glass Transition Temperature	1.3
$\alpha$	Material Loss Parameter	1.6.2
$^{\circ}\text{C}$	Operating Temperature	3.3.3
$M_w$	Melt Flow Index	3.5.2
$\mu_0$	Magnetic Permeability in free space	4.2
$\epsilon_0$	Dielectric Constant	4.2
$\epsilon(\mathbf{r})$	Relative Dielectric Constant	4.2
$D(\mathbf{r}, t)$	Electric Displacement	4.2
$\mathbf{a}_i$	Elementary Lattice Vector	4.2
$\mathbf{b}_i$	Elementary Reciprocal Lattice Vector	4.2
$\mathbf{l}_i$	Arbitrary Vector	4.2
$\delta_{ij}$	Kronecker's delta	4.2
$c$	Velocity of light in free space	4.2
$\beta$	Phase Propagation Constant	4.3.1
$\lambda_{01}$	Wavelength of the mode	4.3.1
$n_{\text{eff}}$	Effective refractive index	4.3.1
$\lambda$	Vaccum Wavelength	4.3.1
$\alpha_{\text{eff}}$	Effective Material loss	4.3.2
$\beta_2$	Dispersion Parameter	4.3.3
$B$	Birefringence	4.3.4



$V$	Normalized frequency	4.3.1
$L_{con}$	Confinement Loss	4.3.1
$\eta_c$	Power Fraction	4.3.1
$A_{eff}$	Effective Area	4.3.1
$\gamma$	Non-linear Co-efficient	4.3.1
$f$	Operating frequency	4.3.1

# Chapter 1

## INTRODUCTION

### 1.1 Terahertz Radiation and Its Applications

The emerging electromagnetic frequency band ranging from 0.1 THz to 10 THz lying between microwave and infrared band, known as terahertz band [1], has drawn significant attention of researchers in recent years due to its promising applications in the field of non-invasive medical imaging [2], sensing [3], spectroscopy [4], pharmaceutical drug testing, astronomy [5], communication [6], security screening [7], biomedical applications [8,9] and so on.

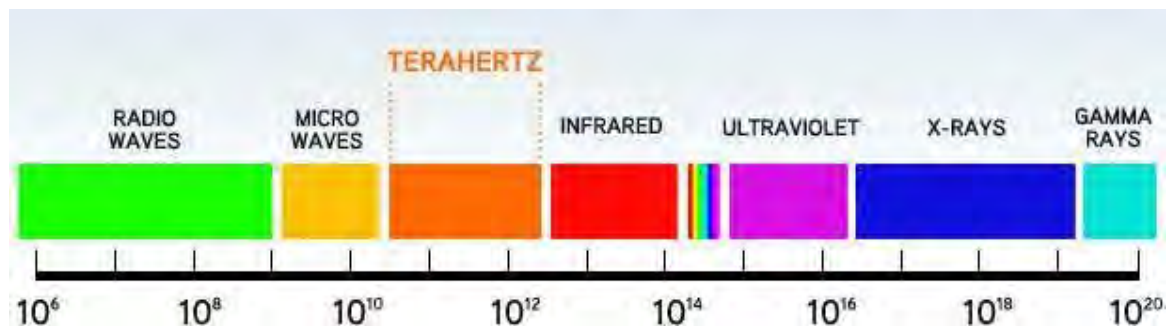


Figure 1.1: Electromagnetic Frequency Spectrum

Basically, a terahertz system mainly consists of THz source, waveguide and the THz detector. Though efficient THz sources and detectors are commercially available in the market, implementation of efficient terahertz waveguides is still a great challenge for the researchers. This is due to the fact that all the existing dielectric materials absorb modal power in THz regime. Transmission of THz wave using free space is unreliable because of path loss, high absorption loss and tough alignment. Hence it is necessary to design efficient waveguides for long distance transmission of the terahertz waves.

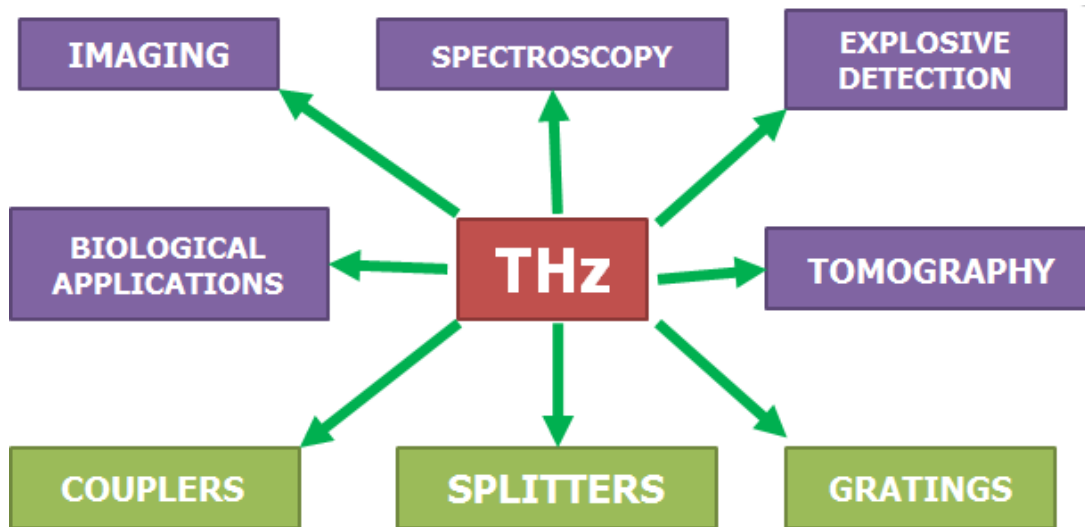


Figure 1.2: Applications of THz waves

## 1.2 Terahertz Waveguides

A waveguide is a device used to carry electromagnetic waves from one place to another without significant loss in intensity while confining them near the propagation axis. The most common type of waveguides for radio waves and microwaves is a hollow metal pipe. Waves propagate through the waveguide, being confined to the interior of the pipe. A representative waveguide in the optical region is an optical fiber. Fiber-optic communication and a variety of other applications exploit the extremely low attenuation and dispersion of silica-based optical fibers in the optical communication band of 1.3-1.6  $\mu\text{m}$ . Several microwave and optical waveguide technologies have been examined in the THz region. The major challenge of THz waveguide technologies is the relatively strong absorption in most of the conventional THz waveguide structures, which prevents THz wave transmission over long distances.

## 1.3 History of Photonic Crystal Fiber Based Terahertz Waveguides

Optical fibers (OFs) development in 1966 revolutionized fields such as telecommunications and sensing, leading to the creation of high sensitivity and controlled systems based on light guidance. The remarkable characteristics of fiber optics such as geometric versatility, increased sensitivity over existing techniques, and inherent compatibility with fiber optic telecommunications technology make them stand out for sensing applications. Optical-fibers-

based sensors [10] are low cost and efficient solutions for several industries due to their high sensitivity, small size, robustness, flexibility, and ability for remote monitoring as well as multiplexing. Other advantages entail their aptitude to be used even in the presence of unfavorable environmental conditions such as noise, strong electromagnetic fields, high voltages, nuclear radiation, in explosive or chemically corrosive media, at high temperatures etc. Even though standard optical fibers present an excellent performance in fiber telecommunications, the intrinsic properties of silica have imposed restrictions in the evolution of this technology. The first evident restriction is the material selection for the core and cladding, in order to have matching thermal, chemical, and optical properties. Other limitations are related to its geometry and refractive index profile, which do not allow for freely engineering of optical fiber characteristics such as inherent losses, dispersion, nonlinearity, and birefringence in order to progress in applications such as high power lasers or fiber sensors etc. These limitations and restrictions have been refined during 30 years of exhaustive research, taking fiber optic technology nearly as far as it could go.

The introduction of photonic crystal fibers (PCFs) [11] in 1996 was a breakthrough in fiber optic technology given that these fibers not only had unprecedented properties as they could overcome many limitations intrinsic to standard optical fibers. Photonic crystal fiber geometry is characterized by a periodic arrangement of air holes running along the entire length of the fiber, centered on a solid or hollow core. The major difference between both kinds of fibers relies on the fact that the waveguide properties of photonic crystal fibers are not from spatially varying glass composition, as in conventional optical fiber, but from an arrangement of very tiny and closely spaced air holes which go through the whole length of fiber. In contrast with standard optical fibers, photonic crystal fibers can be made of a single material and have several geometric parameters which can be manipulated offering large flexibility of design. Furthermore, these fibers offer also the possibility of light guiding in a hollow core, opening new perspectives in fields such as nonlinear fiber optics, fiber lasers, super-continuum generation, particle guidance, and fiber sensors. Therefore, there is a high interest of the scientific community in employing photonic crystal fibers in all kind of fields.

There are several materials available that can be used to design terahertz waveguides. Such materials include polymethyl-methacrylate (PMMA), High density polyethylene (HDPE), Teflon [12], Topas [13–16] etc. Most of the recent simulation and experimental works on

THz waveguides have been performed taking Topas as background material due to its several unique favorable qualities such as low water absorption, low material absorption loss ( $0.2 \text{ cm}^{-1}$ ), much higher glass transition temperature ( $T_g$ ) than PMMA, good for bio-sensing. Moreover, its constant refractive index (1.535) over a wide terahertz frequency band makes the chromatic dispersion negligible. However, we choose a latest cyclo-olefin polymer (COP) named as Zeonex [17–19] as the background material for our proposed model because of its unique advantages over Topas including lower content of impurities, higher heat resistance, lower dielectric constant and loss tangent. Moreover, it has lower specific gravity, chemical resistance at elevated temperature, higher transparency, lower melt flow index etc. Furthermore, the physical properties of Zeonex [20] are also suitable for high quality fiber drawing compared to Topas. Also, fluctuations in the fiber diameter are reduced because of the greater stability of drawing process. This allows more degrees of freedom in fiber design. In addition, it offers a wide range of drawing stress which makes the fabrication much easier.

#### **1.4 Applications of PCF Based Terahertz Waveguides**

Their special properties make photonic crystal fibers very attractive for a very wide range of applications. Some examples are:

- fiber lasers and amplifiers, including high-power devices, mode-locked fiber lasers, etc.
- nonlinear devices e.g. for super continuum generation, Raman conversion, parametric amplification, or pulse compression.
- telecom components, e.g. for dispersion control, filtering or switching.
- fiber-optic sensors of various kinds.
- quantum optics, e.g. generation of correlated photon pairs, electromagnetically induced transparency, or guidance of cold atoms.

Even though PCFs have been around for several years, the huge range of possible applications is far from being fully explored. It is to be expected that, this field will stay very lively for many years and many opportunities for further creative work, concerning both fiber designs and applications.

## 1.5 Characterization of THz Waveguides

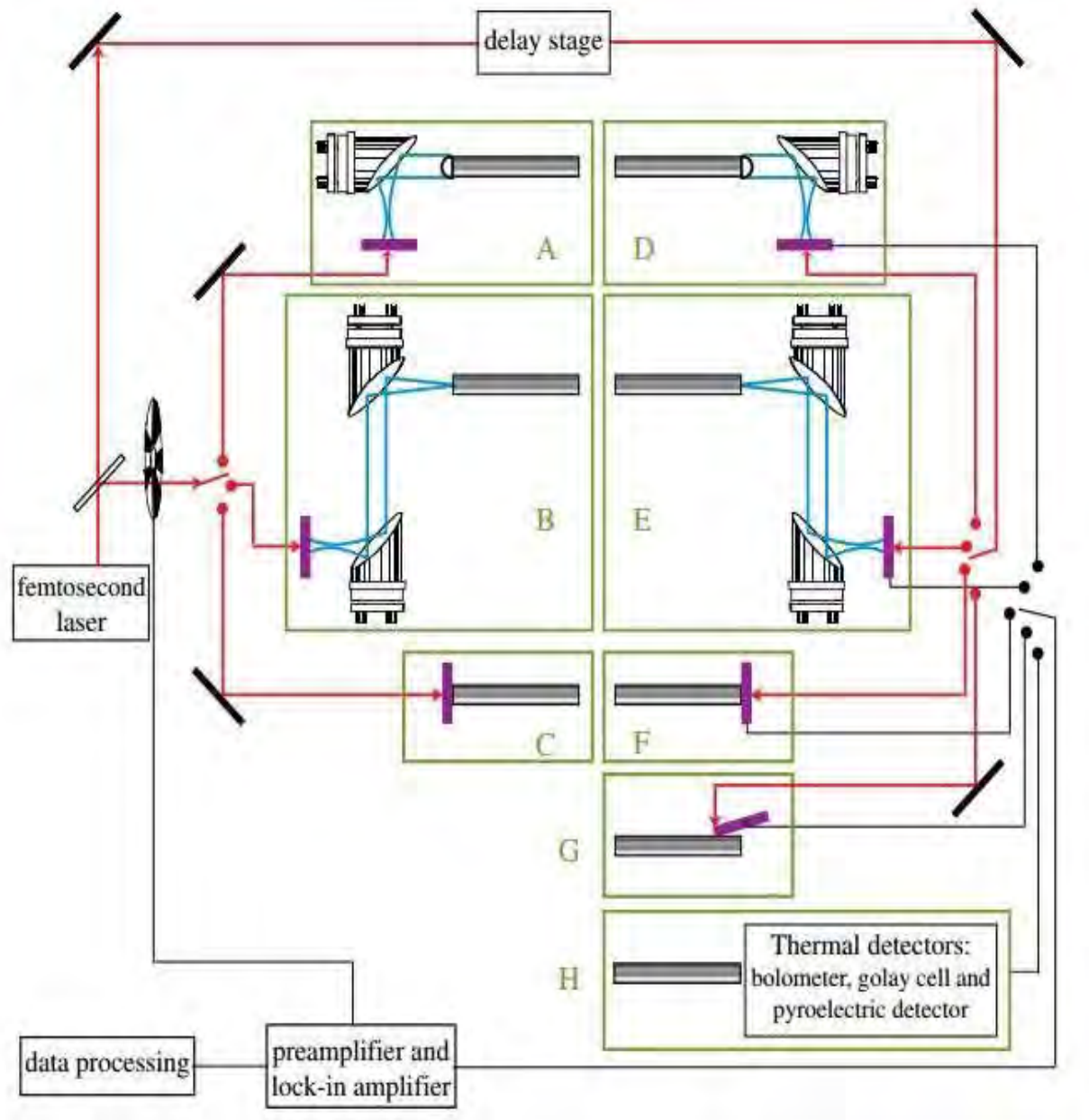
The term waveguide characterization [21] is used to imply the study of the loss and dispersion properties of the waveguide as a function of frequency/ wavelength. Different arrangements of emitters, detectors, and THz optics (mirrors and lenses) can be utilized for characterization of a THz waveguide, which is summarized in Fig. 1.3. Usually photoconductive antennas and nonlinear crystals are employed in the generation of THz pulses. The generated THz pulses are typically manipulated and focused employing parabolic mirrors and silicon/dielectric lenses, as seen in options A and B in Fig. 1.3. Silicon/dielectric lenses are used at the interface of the waveguide to achieve a smaller spot size at the front-end of the waveguide and consequently to increase the coupling into the waveguide. An alternative approach is positioning the waveguide on the emitter, shown by option C in Fig. 1.3, for coupling into the waveguide. As an example, McGowan et al. and Mendis [22] and Grischkowsky used option A, Chen et al., Ponseca et al. and Lai et al. used option B, and Jeon et al., Wächter et al. , and Atakaramians et al. used option C for coupling THz pulses into the waveguides.

Similar arrangements to those used to couple into the waveguides are employed for coupling out the THz pulses from the waveguide, as shown in the right hand side (options D to F) of Fig. 1.3. Development of near-field photoconductive probes has not only advanced THz near-field imaging, but has also allowed probing THz pulses along the waveguides. This approach, shown in option G in Fig. 1.3, is suitable for waveguides that have extended power outside the structure where the probe-tips can be positioned. As an example, McGowan et al., Gallot et al., and Mendis and Grischkowsky used option D, Ponseca et al. used option E, Jeon et al. and Wang and Mittleman used option F, and Wächter et al. and Atakaramians et al. used option G for coupling THz pulses into the waveguides. All the detection methods (options D to G) discussed so far employ photoconductive detectors for measuring THz pulses. This approach is known as coherent detection. In this approach both the amplitude and the phase of the electric field and consequently the absorption coefficient (effective material loss) and effective refractive index of the propagating mode can be determined as a function of frequency. The relevant equations are discussed later in this section. Thermal detectors (e.g., bolometer and pyroelectric devices) are also employed to measure the

intensity of the THz radiation, from which only the absorption coefficient of the propagating mode can be determined as a function of frequency. As an example, Chen et al., Bowden et al., and Lai et al. used the thermal detection method (option H in Fig. 1.3) for coupling THz pulses into the waveguides.

The standard generation and coupling in techniques are shown in the left hand side of the figure (options A to C), while the detection and coupling out techniques are shown in the right-hand side of the figure (options D to H). Any combination of options A to C and options D to H in Fig. 1.3 can be used for the characterization of THz waveguides. The waveguides are mostly characterized in transmission mode; i.e., the THz pulse is launched into the waveguide from one end and coupled out and measured from the other end. To date only one reflection mode characterization technique has been reported, where the THz pulses are coupled into and out of the fiber from one end, and a metal plate is positioned at the end of the fiber to reflect the beam.

In general, two different methods have been used for the characterization of THz waveguides. In the first approach, two pulses are measured: a reference pulse when all the steering and coupling devices are in the system except the waveguide and a sample pulse when the waveguide is also included in the system. The loss and dispersion parameters are calculated from these two measurements. For example, have used this approach for characterization of THz waveguides. In the second approach, THz pulses propagating through a minimum of two different lengths of a waveguide are measured and compared, where the loss and dispersion parameters are calculated. This method for characterization of waveguides is known as the cut-back technique and is used primarily for characterization of fibers in optics. In this technique the waveguide is situated in the system and the propagating pulses are measured at the output. Later the waveguide is cut down from the output end so that the coupling in arrangement is maintained and the propagating pulses are measured once more. This can be repeated as many times as desired. Since the waveguide is cut down for each measurement, this technique is called the cut-back technique. For example, have used this approach for characterization of THz waveguides.



legend

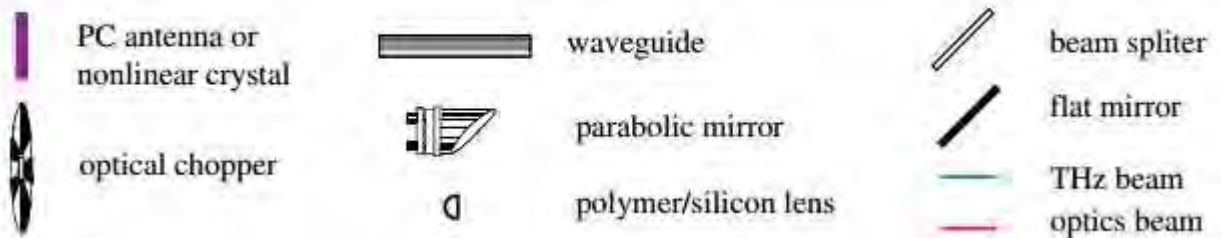


Figure 1.3: Schematic of the devices required for characterization of THz waveguides.



## 1.6 Classifications of THz Waveguides

Different types of THz waveguide are already experimented. All of those can be divided in two types according to the material used.

### 1.6.1 Metallic waveguides

Metallic waveguides[23] proposed for THz radiation guidance are mostly scaled down versions (in terms of dimension) of well-known guiding devices from microwave and radio frequencies. The electromagnetic waves at THz frequencies are not as dissipative in metallic components as they are for higher frequencies such as visible light. Thus metallic structures still can be used for guidance in this regime. Hollow metallic circular/rectangular waveguides [23], parallel-plate waveguides, coaxial waveguides, metal wire waveguides [24], parallel-plate photonic waveguides, metal sheet waveguides, and metallic slot waveguides are examples of metallic waveguides proposed for guidance of the THz spectrum.

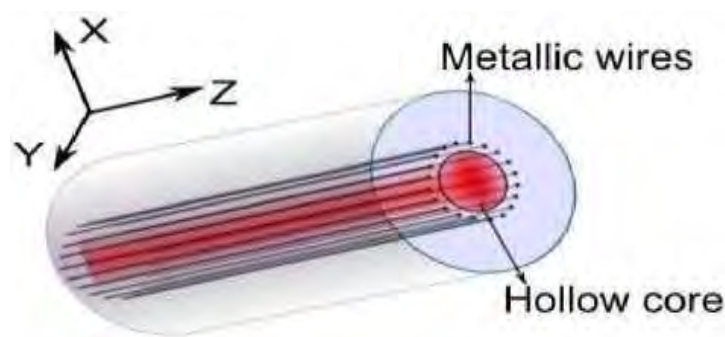


Figure 1.4: Hollow core metallic waveguide

### 1.6.2 Dielectric waveguides

Another major category of non-planar waveguides proposed for the THz spectrum is dielectric waveguides [25]. These waveguides are also known as fibers if they are flexible and have circular cross sections and are mostly used at higher frequencies, such as IR and optical frequencies, where metallic waveguides are dissipative.

Dielectric waveguides suffer from material absorption since suitable dielectric materials for fabrication of waveguides are lossy. Although high-resistivity silicon has extremely low loss

( $\alpha < 0.05 \text{ cm}^{-1}$  for frequencies below 2.5 THz), it is not amenable for fabrication of many waveguide geometries. The material choice and waveguide structure have a great impact on the waveguide performance, not only on transmission loss but also on dispersion.

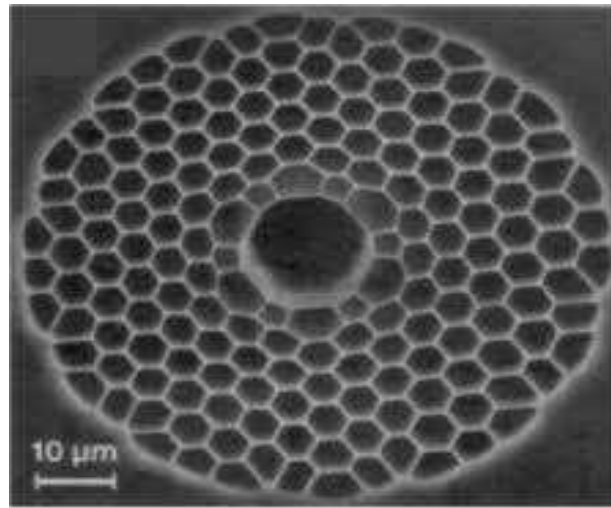


Figure 1.5: Circular dielectric waveguide

The dielectric waveguides proposed for THz guidance can be divided into three classes: hollow-core [26–28], solid-core [29], and porous-core [30,31–37] waveguides. The guiding mechanism for each class of structure is different. The guiding mechanisms in all-dielectric hollow-core waveguides come from formation of either photonic bandgaps or anti-resonances with the immediate cladding structure. If the waveguides have an inner metallic coating, then the mode is guided via reflection from the metal coating, which presents a highly reflective mirror. On the other hand, the guiding mechanisms in solid-core and porous-core waveguides are based on total internal reflection if the average refractive index of the core is greater than that of the cladding (e.g., air-clad). When the average refractive index of the core is smaller than that of the cladding, the guiding mechanisms via formation of the photonic bandgap.

The fabrication process of dielectric waveguides has benefited from the advance fabrication process of optical waveguides, especially microstructured optical fibers [16,18,38–41] (MOFs) and IR waveguides. The fabrication techniques for MOFs usually have two stages. The first stage is the fabrication of a fiber preform, which is the scaled-up version of the fiber. In the second stage, the fiber preforms are drawn to fibers often via a caning stage to provide a central core region with smaller scale structure. There are a range of techniques available for fabrication of MOF preforms: stacking of capillary tubes, drilling holes in the

bulk material, casting into a microstructured mold, and extrusion. On some occasions, due to the larger dimension of THz waveguides compared to that in the optics, the fabrication of waveguides encountered fewer steps. As we shall observe in this section, for THz hollow-core and solid-core microstructured waveguides, the waveguide preforms by itself is suitable for THz guidance, resulting in the elimination of the second stage in the fabrication process, i.e., the drawing process. In the area of fabrication of THz waveguides, there are also some techniques borrowed from fabrication of hollow-core IR waveguides, e.g., using a sputtering ring chamber or wet-chemistry technique to deposit metallic/dielectric layers on/inside a tube.

## **1.7 Motivation of the Work**

Due to the immense popularity, THz wave generation and detection have been flourished promisingly in the last decades. However, free space propagation is preferred for existing THz systems as all the existing materials for guiding the THz waves are extremely absorbent in this frequency band. Although air in the free space is considered to be non-absorbent, the existing oxygen and water vapor in the air absorb the terahertz signals. Therefore, attention was shifted towards the improvement of various types of terahertz waveguides. A lot of papers on terahertz using several background materials such as Polymethyl Methacrylate (PMMA), High density polyethylene (HDPE), Topas, Teflon, Zeonex etc. have been proposed so far. However, Zeonex has several favorable characteristics over other dielectric materials such as lower content of impurities, higher heat resistance, lower dielectric constant and loss tangent. Moreover, it has lower specific gravity, higher chemical resistance at elevated temperature, higher transparency etc. Furthermore, lower melt flow index of Zeonex is very suitable for high quality fiber drawing [18] compared to other polymer dielectric materials. Also, fluctuations in the fiber diameter are reduced because of the greater stability of drawing process. This allows more degrees of freedom in fiber design. In addition, it offers a wide range of drawing stress which makes the fabrication much easier.

Hence, there is still a great scope to improve the various modal characteristics of porous core THz fibers using Zeonex as the background material.

## **1.8 Objectives with Specific Aims and Possible Outcome**

The objectives of this work are:

- I. To design and optimize a Zeonex based porous core fiber with very high birefringence and low absorption loss for the efficient guidance of THz waves.
- II. To simulate the design to obtain various desirable modal characteristics of the fiber.

The possible outcome is a novel Zeonex based waveguide with much higher birefringence and lower absorption loss that can be used in polarization preserving applications such as sensing and optical coherent communications etc.

## **1.9 Organization of the Thesis**

The thesis consists of six parts.

Chapter 1 contains introductory discussion on THz radiation, Applications of THz waves, THz waveguides and their types. Motivation and objective of this thesis work are also presented here.

In chapter 2, we put our focus on THz sources and detectors. Various types of THz sources and detectors are discussed in this section.

In chapter 3, Background materials for THz guidance are discussed. It also covers advantages, disadvantages and different properties such as refractive index, specific gravity, loss tangent, tensile strength, water absorption etc of THz waveguides.

Chapter 4 represents the theoretical physics, analysis, Finite element method to solve the Helmholtz equation of electromagnetic waves to determine various wave-guiding parameters of THz fibers. It also covers different characteristic parameters like refractive index, absorption loss, dispersion, power fraction, non-linearity etc.

Chapter 5 includes proposed design and simulation procedures. It also contains the comparison table with some previous and contemporary works.

Chapter 6 is the concluding chapter. It contains the summary of our work along with the highlights on the future scope of our work. All references are placed at the end of our thesis.

# Chapter 2

## TERAHERTZ SOURCES AND DETECTORS

### 2.1 Introduction

Basically, a terahertz system mainly consists of THz source, waveguide and the THz detector. For a long time, terahertz radiation was little used in science and technology, essentially since there were neither good terahertz sources nor suitable detectors available. Therefore, this spectral range was often called the terahertz gap. This gradually changed until in the 1990s the interest in terahertz waves grew strongly, and more and more research groups engaged in this area. The rapid advances in that field are largely due to advances in photonics, which created various powerful solutions both for generation and detection of terahertz waves. These advances have strengthened the motivation for further efforts in various areas of terahertz technology, and the fast increasing technological options also open a wide field of applications.

Though efficient THz sources and detectors are commercially available in the market now-a-days, implementation of efficient terahertz waveguides is still a great challenge for the efficient transmission of THz waves. This is due to the fact that all the existing dielectric materials absorb modal power in THz regime. Transmission of THz wave using free space is unreliable because of path loss, high absorption loss and tough alignment. Hence, it is necessary to design efficient waveguides for long distance transmission of the terahertz waves.

### 2.2 Terahertz Sources

There are several techniques available to generate terahertz waves. Some of the techniques are discussed below.

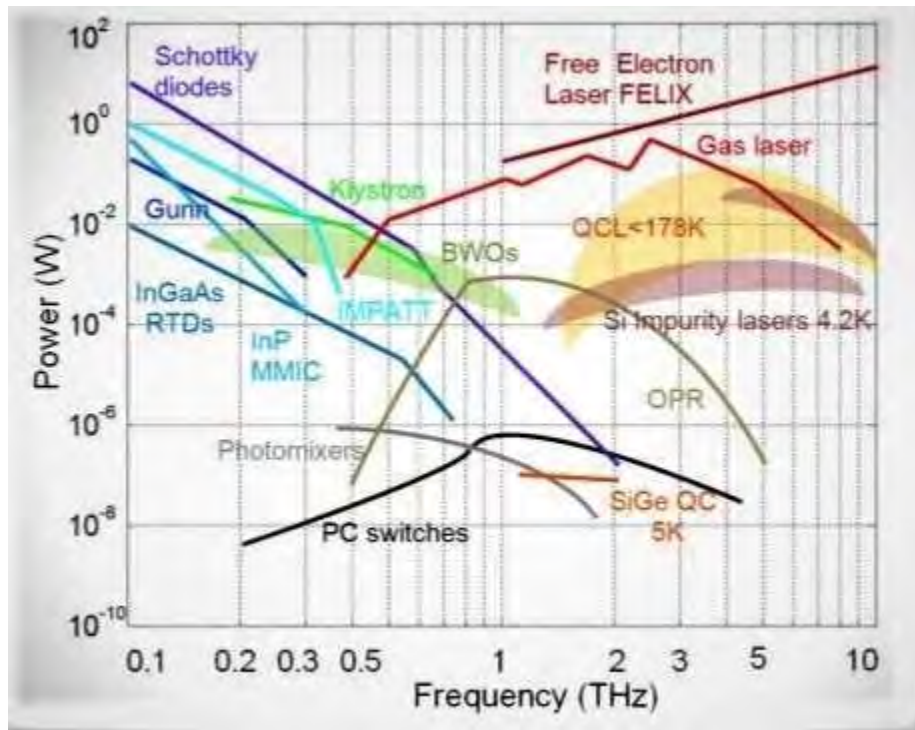


Figure 2.1: THz sources[42]

### 2.2.1 Gas lasers

Certain molecular gas lasers can generate terahertz radiation. (They are also called far infrared lasers.) They exploit transitions of certain molecules (e.g. of methanol) between rotational states, with which discrete frequencies in a wide range can be generated typically with output powers of a few milliwatts or some tens of milliwatts. Such gas lasers are usually optically pumped, e.g. with a CO<sub>2</sub> laser. The conversion efficiency is very low.

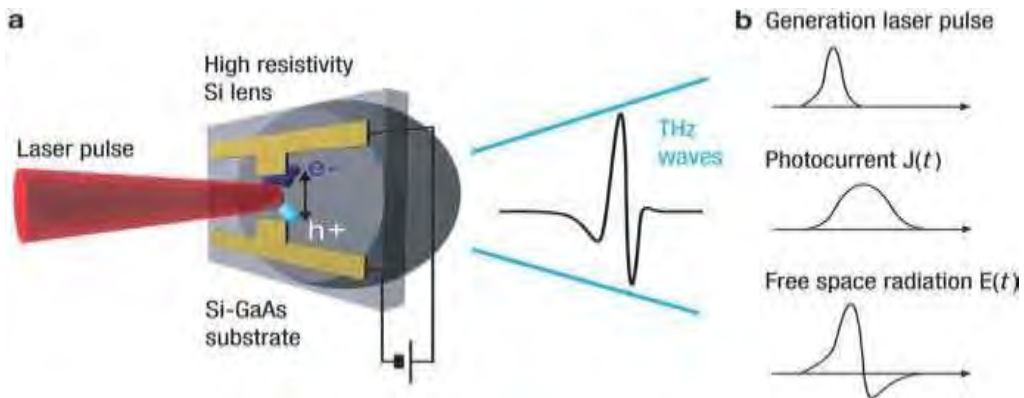


Figure 2.2: Gas Laser[42]

### **2.2.2 Sources derived from microwave technology**

Microwave technology presents a number of options for high-frequency oscillators, such as Gunn diodes, Impatt diodes and resonant tunneling diodes. Some of these have been optimized long ago for emitting at particularly high frequencies up several terahertz. In that regime, however, the performance is much lower than at lower frequencies.

Another way to obtain higher frequencies is harmonic generation in nonlinear electronic devices. This requires high-power pump sources and typically delivers rather low output powers. Generally, the performance of such microwave technology sources is quite moderate in terms of output power and spectral coverage.

### **2.2.3 Free-electron lasers and synchrotrons**

Free electron lasers as well as synchrotron light sources can be constructed which emit very high powers in the terahertz spectral regions. They are useful for various research purposes, but are very large and expensive. Therefore, they have quite limited use for general terahertz technology.

### **2.2.4 Photoconductive antenna**

In the area of optical sampling technology, photoconductive dipole antennas have been developed which are suitable both for generation and detection of high-frequency electromagnetic signals. Miniature versions of such antennas allowed their use also in the terahertz region. Essentially, a sender antenna consists of two short metallic stripes with a small gap in between, made on a semiconductor material with a short charge carrier lifetime. A DC bias voltage is applied to the stripes, and an intense ultrashort laser pulse from a mode-locked laser focused on the region between the metallic stripes generates a short circuit for a short time. (The semiconductor gap serves as a photoconductive switch.) The fast potential change induces fast oscillations in the antenna, which in turn lead to terahertz radiation emitted in a wide range of angles.



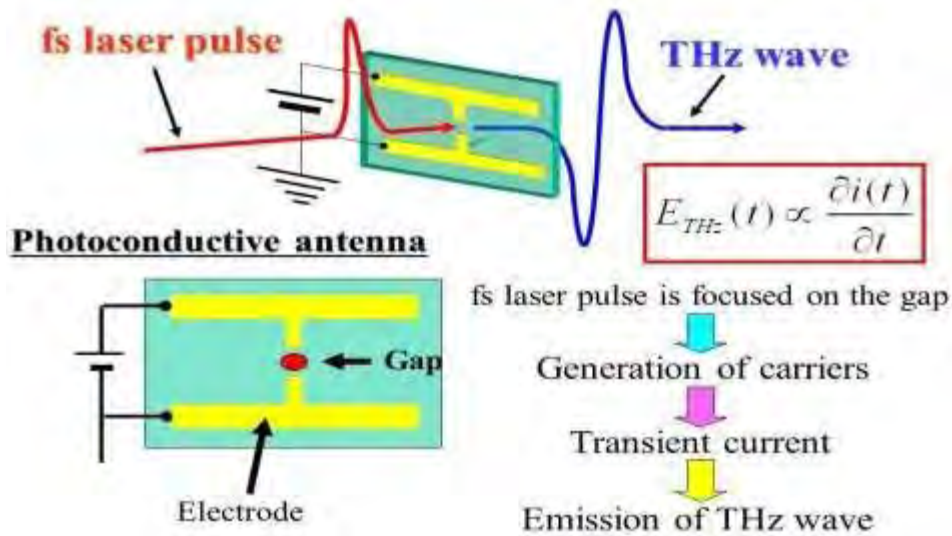


Figure 2.3: Photoconductive Antenna as THz source[42]

The decay is often so fast that one obtains a single-cycle source, i.e., a source emitting only about a single cycle of the electromagnetic oscillation. The emission spectrum may then roughly cover a substantial part of an octave or even more. This can be useful for spectroscopy, for example, as it allows one to cover a large frequency range without needing a tunable source.

For higher output powers, devices with larger areas have been constructed with interdigitated electrodes as part of a metal–semiconductor–metal (MSM) structure.

Photoconductive antennas can also be operated in a continuous-wave mode where irradiation is done with two single-frequency laser diodes (or with a single two-color laser), having a terahertz different frequency. Particularly in that continuous-wave regime, photoconductive antennas are also called terahertz photomixers.

### 2.2.5 Parametric interactions in nonlinear crystals

One can use difference frequency generation of two optical waves with similar frequency to obtain terahertz radiation. Alternatively, one may have two frequency components of a broadband ultra-short pulse interacting nonlinearly. Such processes are possible not only in photo-mixers as discussed above, but also in various nonlinear crystal materials and essentially work like difference frequency generation for mid-infrared laser sources, for

example. If only a single input beam (not a dual-frequency source) is used, the method is called optical rectification. This is explained in detail in the corresponding encyclopedia article.

### 2.2.6 Optical rectification in gases

Somewhat surprisingly, optical rectification of femtosecond optical pulses, leading to terahertz wave emission, can also occur in a gas (e.g. air). Here, a plasma is generated by the superposition of an infrared beam with its second harmonic. Careful phase control of the involved waves is necessary for a high conversion efficiency. Compared with optical rectification in crystals, the emission bandwidth is typically higher, and higher pulse energies can be obtained.

### 2.2.7 Quantum cascade lasers

Quantum cascade lasers are semiconductor lasers which have originally been developed for emitting in the mid- and far-infrared spectral region. Optimization for particularly long emission wavelength has lead to emission frequencies of only a few terahertz, which may be tuned in some limited range. Such lasers are very compact, but need a cryogenic cooling system.

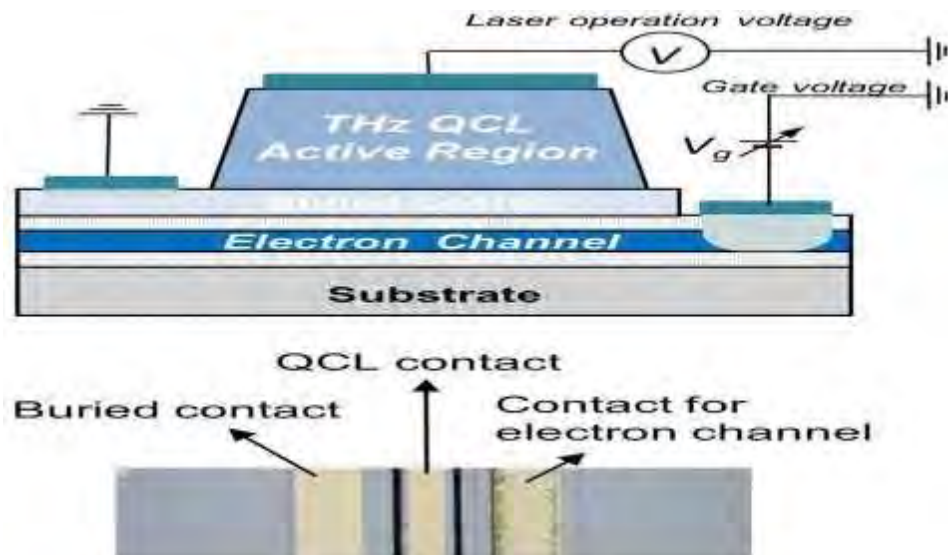


Figure 2.4: Quantum Cascade Laser[42]

## 2.3 Terahertz Detectors

Terahertz (THz) detectors play an important role in different areas of human activities (e.g., security, biological, drugs and explosions detection, imaging, astronomy applications, etc.). In the section, issues associated with THz detectors will be discussed.

### 2.3.1 Photoconductive antenna

Photoconductive antenna can be used not only for generation of terahertz waves (see above), but also for their detection. Essentially, a kind of pump-probe measurements can be performed, where an optical probe pulse acts on a photoconductive switch while the terahertz wave to be detected passes it. The voltage between the two electrodes of the switch will thereafter be proportional to the electric field of the terahertz wave at the time of the arrival of the probe pulse.

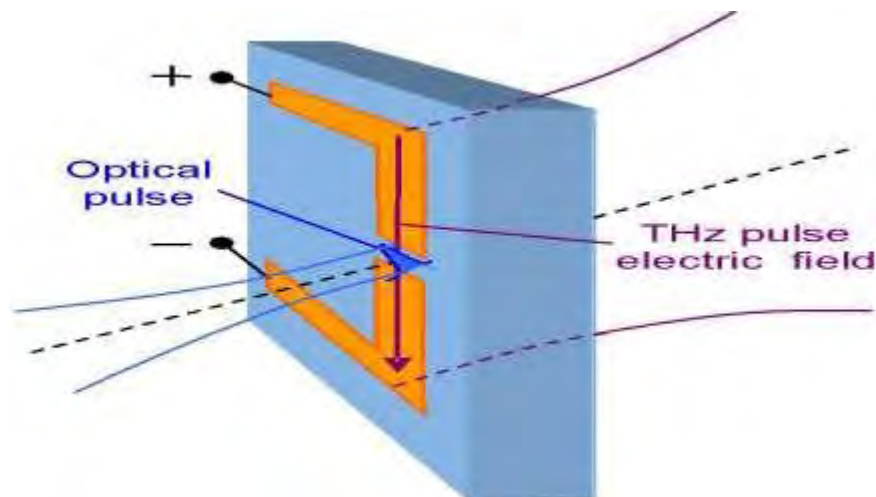


Figure 2.5: Photoconductive Antenna as THz detector[42]

### 2.3.2 Electro-optic sampling

A terahertz wave and an optical field can interact with each other when meeting in a nonlinear crystal material. This effect can be used for the detection of terahertz waves. A frequently used method is time-domain spectroscopy.

### **2.3.3 Bolometers**

Bolometers can be used to detect various forms of radiation based on the heat generated upon absorption. This principle can also be applied to terahertz waves. For example, indium antimonide (InSb) bolometers can be used.

## **2.4 Conclusion**

The two most commonly used methods of T-ray generation are based on photoconductive antenna (PCA) and optical rectification (OR). These two methods are used widely in the field of T-ray spectroscopy. Moreover, due to the advancement of technology now-a-days lots of efficient terahertz detectors are also introduced. These terahertz sources and detectors are most commonly used in science, medicine, imaging and engineering applications.

# Chapter 3

## TERAHERTZ WAVEGUIDE MATERIALS

### 3.1 Introduction

In this chapter, we will discuss about the background materials used for terahertz waveguides. Normally for the propagation of wave in total internal reflection method, we need two different materials for core and cladding respectively. Between two, cladding needs to have lower effective refractive index than core according to the theory. However, we will discuss about advantages, disadvantages and various properties of different polymer materials in this chapter.

### 3.2 Polymethylmethacrylate or PMMA

A transparent thermoplastic, Polymethylmethacrylate (PMMA) [43] is a possible lightweight, shatter-resistant substitute for glass. Often referred to as acrylic glass, PMMA is a synthetic polymer of the organic compound methyl methacrylate (MMA). It is seen as a cheap alternative to polycarbonate when high strength is not necessarily a stringent requirement for the given application. PMMA in its unmodified form can be brittle with particularly poor impact toughness and has a lower hardness than conventional glass rendering it prone to scratches. However, when modified, both of these properties can be significantly improved.

#### 3.2.1 Advantages and disadvantages of PMMA

##### **Advantages:**

There are a number of advantages of using PMMA:

- Outstanding weathering and resistance to UV radiation
- Transparent
- High gloss and hardness (when modified)

- Good rigidity
- Dimensionally stable
- Good abrasion resistance - surface scratches can be polished out (when modified)

**Disadvantages:**

Among several disadvantages the followings are noteworthy:

- Not a tough material in comparison with engineering plastics - notch sensitive and generally brittle
- Although not attacked by alcohol alone, alcohol with carbon tetrachloride and ether will cause swelling
- Dissolved by most aromatic and chlorinated hydrocarbons
- Water absorption is low but can have a considerable effect on dimensions and a lesser one on mechanical properties

**3.2.2 Properties of PMMA [43]**

Density (g/cm <sup>3</sup> )	1.18
Surface Hardness	RM92
Tensile Strength (MPa)	70
Flexural Modulus (GPa)	2.9
Notched Izod (kJ/m)	0.02
Linear expansion (/°C x 10 <sup>-5</sup> )	7
Elongation at Break (%)	2.5
Strain at Yield (%)	N/A
Max. Operating Temp. (°C)	50
Water Absorption (%)	0.3
Oxygen Index (%)	19
Flammability UL94	HB
Volume Resistivity (log ohm.cm)	15
Dielectric Strength (MV/m)	25

Dissipation Factor 1kHz	0.03
Dielectric const. 1kHz	3.3
HDT @ 0.45 MPa (°C)	103
HDT @ 1.80 MPa (°C)	95
Material. Drying hrs @ (°C)	2 @ 75
Melting Temp. Range (°C)	220 - 240
Mould Shrinkage (%)	0.6
Mould Temp. Range (°C)	60 - 80

Table 3-1: Properties of PMMA

### 3.3 High Density Polyethylene or HDPE

High-density polyethylene (HDPE) [44,45] or polyethylene high-density (PEHD) is a polyethylene thermoplastic made from petroleum. It is sometimes called "alkathene" or "polythene" when used for pipes. With a high strength-to-density ratio, HDPE is used in the production of plastic bottles, corrosion-resistant piping, geomembranes, and plastic lumber. HDPE is commonly recycled, and has the number "2" as its resin identification code.

#### 3.3.1 Advantages and disadvantages of HDPE

##### Advantages:

- Low cost
- Impact resistant from -40 C to 90 C
- Moisture resistance
- Good chemical resistance
- Food grades available
- Readily processed by all thermoplastic methods

##### Disadvantages:

- High thermal expansion

- Poor weathering resistance
- Subject to stress cracking
- Difficult to bond
- Flammable
- Poor temperature capability

### 3.3.2 Properties of HDPE [45]

Density (g/cm <sup>3</sup> )	0.96
Surface Hardness	SD68
Tensile Strength (MPa)	30
Flexural Modulus (GPa)	1.25
Notched Izod (kJ/m)	0.15
Linear Expansion (/°C x 10 <sup>-5</sup> )	12
Elongation at Break (%)	100
Strain at Yield (%)	12
Max. Operating Temp. (°C)	55
Water Absorption (%)	0.02
Oxygen Index (%)	17
Flammability UL94	HB
Volume Resistivity (log ohm.cm)	17
Dielectric Strength (MV/m)	21
Dissipation Factor 1kHz	0.001
Dielectric Constant 1kHz	2.5
HDT @ 0.45 MPa (°C)	75
HDT @ 1.80 MPa (°C)	46
Material. Drying hrs @ (°C)	NA
Melting Temp. Range (°C)	220 - 310
Mould Shrinkage (%)	3
Mould Temp. Range (°C)	30 - 70

Table 3-2: Properties of HDPE



### 3.4 Teflon

Teflon [46] is also known as polytetrafluoroethylene (PTFE) and it is a synthetic polymer. This means it is a man-made chemical made up of two main atoms: carbon and fluorine. It is made by polymerizing many tetra-fluoro-ethylene (TFE) molecules together. Polymerization is a process in which molecules are combined into long strands. The TFE molecules are made up of fluorspar, hydrofluoric acid, and chloroform. These chemicals are combined under extreme heat in a process called pyrolysis. Since TFE is extremely flammable it is stored as a liquid, at a low temperature and pressure until it can be polymerized by the PTFE manufacturers. Once it is polymerized, it becomes resistant to other chemicals.

#### 3.4.1 Advantages and disadvantages of Teflon

##### Advantages:

- Outstanding chemical resistance.
- Low coefficient of friction.
- High continuous use temperature (c 180 °C/360 °F).
- Very high oxygen index.

##### Disadvantages:

- High cost. Low strength and stiffness.
- Cannot be melt processed.
- Poor radiation resistance.

#### 3.4.2 Properties of Teflon [46]

Density (g/cm <sup>3</sup> )	2.15
Surface Hardness	SD63
Tensile Strength (MPa)	25
Flexural Modulus (GPa)	0.70
Notched Izod (kJ/m)	0.16
Linear Expansion (/°C x 10 <sup>-5</sup> )	15

Elongation at Break (%)	400
Strain at Yield (%)	70
Max. Operating Temp. (°C)	180
Water Absorption (%)	0.01
Oxygen Index (%)	95
Flammability UL94	V0
Volume Resistivity (log ohm.cm)	18
Dielectric Strength (MV/m)	45
Dissipation Factor 1 kHz	0.0001
Dielectric Constant 1 kHz	2.1
HDT @ 0.45 MPa (°C)	121
HDT @ 1.80 MPa (°C)	54
Material. Drying hrs @ (°C)	NA
Melting Temp. Range (°C)	NA
Mould Shrinkage (%)	NA
Mould Temp. Range (°C)	NA

Table 3-3: Properties of Teflon

### 3.5 Topas

TOPAS cyclic olefin copolymers are ultra-pure, crystal-clear materials with a wide range of unique properties. TOPAS® COC is the trade name for TOPAS Advanced Polymers' cyclic olefin copolymers (COC). The TOPAS® COC family, in contrast to the partially crystalline polyolefins PE and PP, consists of amorphous, transparent copolymers based on cyclic olefins and linear olefins. Cyclic olefin copolymers are a new class of polymeric materials with property profiles which can be varied over a wide range during polymerization.

#### 3.5.1 Advantages and disadvantages of Topas

##### Advantages:

- Superior moisture barrier and low moisture absorption
- Easy thermoformability

- High rigidity and strength
- Dimensional stability
- Excellent purity and low extractables
- Resistance to hydrolysis and many acids, bases and polar organic solvents
- High light transmission, even into the near UV range
- Compatibility with common sterilization methods
- Low water uptake
- Low birefringence
- Very good metallizability
- High surface replication
- High-temperature resistance

**Disadvantages:**

- Higher flowability
- Higher melt flow index ( $M_w$ )
- Fluctuation during fabrication

**3.5.2 Properties of Topas**

Specific gravity (gm/cc)	3.55
Water absorption (24 h immersion in water at 23 °C)	<0.01
Light transmittance (2 mm wall thickness)	91
Refractive index	1.53
Heat distortion temperature (°C)	75
Dielectric loss tangent	0.0003
Dielectric constant	2.19
Tensile strength (MPa)	63

Table 3-4: Properties of Topas

### 3.6 Zeonex

Zeonex [20], a Cyclo Olefin Polymer(COP), is the latest addition in polymer group. Zeonex has a number of several unique qualities including low water absorption, low content of impurities, high heat resistance, low dielectric constant and loss tangent. Moreover, It has low specific gravity, excellent chemical resistance capacity at elevated temperature, high transparency and low absorption loss ( $0.2\text{cm}^{-1}$ ). Its constant refractive index (1.535) over a wide terahertz frequency band causes negligible material dispersion.

#### 3.6.1 Advantages of Zeonex

- Low specific gravity
- High chemical resistance at elevated temperature
- High transparency
- Low absorption loss
- Constant refractive index
- Lower flowability
- High melt flow index ( $M_w$ )
- Less fluctuation during fabrication

#### 3.6.2 Properties of Zeonex [20]

Specific gravity (gm/cc)	1.01
Water absorption (24 h immersion in water at 23 °C)	<0.01
Light transmittance (2 mm wall thickness)	92
Refractive index	1.535
Heat distortion temperature (°C)	132
Dielectric loss tangent	0.0003
Dielectric constant	2.5
Tensile strength (MPa)	70

Table 3-5: Properties of Zeonex

### **3.7 Conclusion**

In this chapter, materials used in fabrication of fibers are discussed. We see that, Zeonex has numerous advantages over other polymer materials. Therefore, we can use it as the background material for the upcoming waveguides.

# Chapter 4

## THEORETICAL ANALYSIS OF THZ FIBERS

### 4.1 Introduction

This chapter will discuss the basic concepts and theories that form the foundation for understanding the unique characteristics of THz radiation and its interaction with materials. Classical electromagnetic theory provides a general description of THz waves which propagate in and interact with macroscopically uniform media. The basic framework of quantum theory is utilized to describe elementary excitations at THz frequencies.

### 4.2 Wave Propagation

We begin with Maxwell's equations. Because we are interested in the eigen modes of the radiation field. We assume here that free charges and the electric current are absent. In this case, Maxwell's equations in the most general form are given in M K S units as follows:

$$\nabla \cdot \mathbf{D}(r, t) = 0 \quad (4.1)$$

$$\nabla \cdot \mathbf{B}(r, t) = 0 \quad (4.2)$$

$$\nabla \times \mathbf{E}(r, t) = - \frac{\partial \mathbf{B}(r, t)}{\partial t} \quad (4.3)$$

$$\nabla \times \mathbf{H}(r, t) = \frac{\partial \mathbf{D}(r, t)}{\partial t} \quad (4.4)$$

The standard notations for the electric field ( $\mathbf{E}$ ), the magnetic field ( $\mathbf{H}$ ), the electric displacement ( $\mathbf{D}$ ), and the magnetic induction ( $\mathbf{B}$ ) are used in these equations.

In order to solve the wave equations derived from Maxwell's equations, we need so-called constitutive equations that relate  $\mathbf{D}$  to  $\mathbf{E}$  and  $\mathbf{B}$  to  $\mathbf{H}$ . Since we do not deal with magnetic materials in this chapter, we assume that the magnetic permeability of the photonic crystal is equal to that in free space,  $\mu_0$ :

$$\mathbf{B}(\mathbf{r}, t) = \mu_0 \mathbf{H}(\mathbf{r}, t) \quad (4.5)$$

As for the dielectric constant, we assume in this chapter that it is real, isotropic, perfectly periodic with respect to the spatial coordinate  $\mathbf{r}$ , and does not depend on frequency. Those cases in which the dielectric constant is complex, has a disorder, or depends on frequency, which are very interesting and important. We denote the dielectric constant of free space by  $\epsilon_0$  and the relative dielectric constant of the photonic crystal by  $\epsilon(\mathbf{r})$ . The electric displacement is thus given by

$$\mathbf{D}(\mathbf{r}, t) = \epsilon_0 \epsilon(\mathbf{r}) \mathbf{E}(\mathbf{r}, t) \quad (4.6)$$

The periodicity of  $\epsilon(\mathbf{r})$  implies

$$\epsilon(\mathbf{r} + \mathbf{a}_i) = \epsilon(\mathbf{r}) \quad (i=1,2,3) \quad (4.7)$$

Where,  $\{\mathbf{a}_i\}$  are the elementary lattice vectors of the photonic crystal. Because of this spatial periodicity, we can expand  $\epsilon^{-1}(\mathbf{r})$  in a Fourier series. For this, we introduce the elementary reciprocal lattice vectors  $\{\mathbf{b}_i; i = 1, 2, 3\}$  and the reciprocal lattice vectors  $\{\mathbf{G}\}$ :

$$\mathbf{a}_i \cdot \mathbf{b}_j = 2\pi \delta_{ij} \quad (4.8)$$

$$\mathbf{G} = l_1 \mathbf{b}_1 + l_2 \mathbf{b}_2 + l_3 \mathbf{b}_3 \quad (4.9)$$

where  $\{l_i\}$  are arbitrary integers and  $\delta_{ij}$  is Kronecker's delta.  $\epsilon^{-1}(\mathbf{r})$  is expressed as

$$\frac{1}{\epsilon(\mathbf{r})} = \sum_{\mathbf{G}} \kappa(\mathbf{G}) \exp(i\mathbf{G} \cdot \mathbf{r}) \quad (4.10)$$

Because we assumed that the dielectric function is real,  $\kappa(-\mathbf{G}) = \kappa^*(\mathbf{G})$ . When we substitute (4.5) and (4.6) into (4.1)–(4.4), we obtain

$$\nabla \cdot \{\epsilon(\mathbf{r}) \mathbf{E}(\mathbf{r}, t)\} = 0 \quad (4.11)$$

$$\nabla \cdot \mathbf{H}(\mathbf{r}, t) = 0 \quad (4.12)$$

$$\nabla \times \mathbf{E}(\mathbf{r}, t) = -\mu_0 \frac{\partial \mathbf{H}(\mathbf{r}, t)}{\partial t} \quad (4.13)$$

$$\nabla \times \mathbf{H}(\mathbf{r}, t) = -\epsilon_0 \epsilon(\mathbf{r}) \frac{\partial \mathbf{E}(\mathbf{r}, t)}{\partial t} \quad (4.14)$$

When we eliminate  $\mathbf{E}(\mathbf{r}, t)$  or  $\mathbf{H}(\mathbf{r}, t)$  in (4.13) and (4.14), we obtain the following wave equations:

$$\frac{1}{\epsilon(\mathbf{r})} \nabla \times \{\nabla \times \mathbf{E}(\mathbf{r}, t)\} = -\frac{1}{c^2} \frac{\partial^2 \mathbf{E}(\mathbf{r}, t)}{\partial t^2} \quad (4.15)$$

$$\nabla \times \left\{ \frac{1}{\epsilon(\mathbf{r})} \nabla \times \mathbf{H}(\mathbf{r}, t) \right\} = -\frac{1}{c^2} \frac{\partial^2 \mathbf{H}(\mathbf{r}, t)}{\partial t^2} \quad (4.16)$$

Where,  $c$  stands for the light velocity in free space:

$$c = \frac{1}{\sqrt{\mu_0 \epsilon_0}} \quad (4.17)$$

Now, we seek the solutions of (4.15) and (4.16) and get

$$\mathbf{E}(r, t) = \mathbf{E}(r)e^{-i\omega t} \quad (4.18)$$

$$\mathbf{H}(r, t) = \mathbf{H}(r)e^{-i\omega t} \quad (4.19)$$

where  $\omega$  is the eigen-angular frequency, and  $\mathbf{E}(r)$  and  $\mathbf{H}(r)$  are the eigen functions of the wave equations.

### 4.3 Finite Element Method

The description of the laws of physics for space- and time-dependent problems are usually expressed in terms of partial differential equations (PDEs). For the vast majority of geometries and problems, these PDEs cannot be solved with analytical methods. Instead, an approximation of the equations can be constructed, typically based upon different types of discretizations. These discretization methods approximate the PDEs with numerical model equations, which can be solved using numerical methods. The solution to the numerical model equations are, in turn, an approximation of the real solution to the PDEs. The finite element method (FEM) [47] is used to compute such approximations.

One of the benefits of using the finite element method is that it offers great freedom in the selection of discretization, both in the elements that may be used to discretize space and the basis functions.

Another benefit of the finite element method is that the theory is well developed. The reason for this is the close relationship between the numerical formulation and the weak formulation of the PDE problem (see the section below). For instance, the theory provides useful error estimates, or bounds for the error, when the numerical model equations are solved on a computer.

Another benefit of the finite element method is its ability to select test and basis functions. It is possible to select test and basis functions that are supported over a very small geometrical region.

Looking back at the history of FEM, the usefulness of the method was first recognized at the start of the 1940s by Richard Courant, a German-American mathematician. While



Courant recognized its application to a range of problems, it took several decades before the approach was applied generally in fields outside of structural mechanics, becoming what it is today.

## 4.4 Characteristic Parameters

After solving for the pointing vector numerically in a simulation software we get the mode field diagram. Mode field diagram are solved for a number of effective index. Different parameters are then deduced from the solution which are used to describe a fiber. These parameters are known as characteristic parameters.

### 4.4.1 Effective refractive index

The rate of change of phase of the fundamental mode propagating along a straight fiber is determined by the phase propagation constant  $\beta$ . It is directly related to the wavelength of the mode  $\lambda_{01}$  by the factor  $2\pi$ , since  $\beta$  gives the increase in phase angle per unit length. Hence:

$$\lambda_{01} = \frac{2\pi}{\beta} \quad (4.20)$$

Moreover, it is convenient to define an effective refractive index for single mode fiber, sometimes referred to as a phase index or normalized phase change coefficient  $n_{eff}$  by the ratio of the propagation constant of the fundamental mode to that of the vacuum propagation constant:

$$n_{eff} = \frac{\beta}{k} \quad (4.21)$$

Hence, the wavelength of the fundamental mode  $\lambda_{01}$  is smaller than the vacuum wavelength  $\lambda$  by the factor  $1/n_{eff}$  where:

$$\lambda_{01} = \frac{\lambda}{n_{eff}} \quad (4.22)$$

It should be noted that the fundamental mode propagates in a medium with a refractive index  $n(r)$  which is dependent on the distance  $r$  from the fiber axis. The effective refractive index can therefore be considered as an average over the refractive index of this medium. Within a normally clad fiber, not depressed-cladded fibers, at long wavelengths (i.e. small  $V$  values) the MFD is large compared to the core diameter and hence the electric field extends far into the cladding region. In this case the propagation constant  $\beta$  will be approximately equal to

$n_2k$  (i.e. the cladding wave number) and the effective index will be similar to the refractive index of the cladding  $n_2$ . Physically, most of the power is transmitted in the cladding material. At short wavelengths, however, the field is concentrated in the core region and the propagation constant  $\beta$  approximates to the maximum wave number  $n_1k$ . Following this discussion, the propagation constant in single-mode fiber varies over the interval  $n_2k < \beta < n_1k$ . Hence, the effective refractive index will vary over the range  $n_2 < n_{eff} < n_1$ .

#### 4.4.2 Normalized frequency or V-parameter

Normalized frequency or  $V$ -parameter is computed to ensure whether the fiber operates at single-mode or multi-mode by the following equation [48]

$$V = \frac{2\pi r f}{c} \sqrt{(n_{co}^2 - n_{cl}^2)} \leq 2.405, \quad (4.23)$$

where,  $r$  is the radius of the core,  $f$  is the operating frequency,  $c$  is the speed of the light in free space,  $n_{co}$  and  $n_{cl}$  are the refractive indices of the fiber core and cladding respectively.  $n_{cl}$  is considered to be nearly 1. It is due to the fact that, cladding is mainly consisted of compact rectangular air-holes and  $n_{co}$  is considered to be  $n_{eff}$  because core has material and air holes. In order to maintain single mode operation, the value of  $V$ -parameter must be equal to or less than 2.405.

#### 4.4.3 Effective material loss

Effective material absorption is a loss mechanism related to the material composition and the fabrication process for the fiber, which results in the dissipation of some of the transmitted optical power as heat in the waveguide. Expression for effective material loss is [49]:

$$\alpha_{eff} = \sqrt{\frac{\epsilon_0}{\mu_0}} \left( \frac{\int_{mat} n_{mat} |E|^2 \alpha_{mat} dA}{|\int_{all} S_z dA|} \right), \text{cm}^{-1} \quad (4.24)$$

where  $\alpha_{mat}$  is the material absorption loss,  $n_{mat}$  is the refractive index of the background material,  $\alpha_{mode}$  is the fundamental mode loss,  $E$  is the modal electric field,  $S_z$  is the z-component of the pointing vector ( $S_z = \frac{1}{2}(\mathbf{E} \times \mathbf{H}^*) \cdot \hat{z}$ ) and  $\epsilon_0$  and  $\mu_0$  are the permittivity and permeability of free space, respectively. The effective material loss mainly depends on the amount of solid background material used in the fiber.

#### 4.4.4 Confinement loss

Another important parameter that determines the performance of the porous-core fiber is the confinement loss. This loss component occurs due to the finite number of air-hole rings used in the cladding and limits the terahertz signal transmission. This loss can be computed by the following equation [50]

$$L_{con} = \left( \frac{4\pi f}{c} \right) \text{Im}(n_{eff}), \text{ cm}^{-1} \quad (4.25)$$

Where,  $L_{con}$ ,  $f$  and  $c$  are defined as the confinement loss, frequency and speed of the light respectively and  $\text{Im}(n_{eff})$  represents the imaginary part of the complex effective refractive index.

#### 4.4.5 Dispersion

The wave guiding of the fiber may also create chromatic dispersion. This results from the variation in group velocity with wavelength for a particular mode. Considering the ray theory approach, it is equivalent to the angle between the ray and the fiber axis varying with wavelength which subsequently leads to a variation in the transmission times for the rays, and hence dispersion. For a single mode whose propagation constant is  $\beta$ , the fiber exhibits waveguide dispersion when  $d^2\beta/d\lambda^2 \neq 0$ . Expression for dispersion is [51]:

$$\beta_2 = \frac{2}{c} \frac{dn_{eff}}{d\omega} + \frac{\omega}{c} \frac{d^2n_{eff}}{d\omega^2}, \text{ ps}^2/\text{THz/cm} \quad (4.24)$$

where,  $\omega = 2\pi f$ ,  $c$  is the velocity of light in vacuum and  $n_{eff}$  is the effective refractive index of the fiber.

#### 4.4.6 Birefringence

Single-mode fibers with nominal circular symmetry about the core axis allow the propagation of two nearly degenerate modes with orthogonal polarizations. They are therefore bimodal supporting  $\text{HE}^x$  and  $\text{HE}^y$  modes where the principal axes  $x$  and  $y$  are determined by the symmetry elements of the fiber cross section. Hence in an optical fiber with an ideal optically circularly symmetric core both polarization modes propagate with identical velocities. Manufactured optical fibers, however, exhibit some birefringence resulting from differences

in the core geometry (i.e. ellipticity) resulting from variations in the internal and external stresses, and fiber bending. The fiber therefore behaves as a birefringent medium due to the difference in the effective refractive indices, and hence phase velocities, for these two orthogonally polarized modes. If  $n_x$  and  $n_y$  are effective index of x and y polarized mode respectively then the expression for phase birefringence is [52]

$$B = |n_x - n_y|, \quad (4.25)$$

Once modal birefringence is known, group birefringence can also be calculated by using the formula [63] given bellow

$$G_B = B - \lambda \frac{dB}{d\lambda}, \quad (4.26)$$

where,  $G_B$  is the group birefringence and ' $\lambda$ ' be the wavelength.

#### 4.4.7 Power fraction

It is much desirable to flow the power through the core air holes of fiber since dry air does not absorb terahertz power. The power fraction ( $\eta$ ) is calculated to determine the amount of power propagated through fiber's different regions. The core power fraction ( $\eta_c$ ) is defined as the fraction of total modal power flowing through the core air holes of the fiber. It can be calculated by the following formula [51]

$$\eta_c = \frac{\int_{core\ air\ holes} S_z dA}{\int_{all} S_z dA}, \quad (4.27)$$

where, the integration in the numerator is over the region of core air holes and the integration in the denominator is over the total fiber region.

#### 4.4.8 Effective area and non-linearity

The area covered by electromagnetic waves in the core region is called effective area ( $A_{eff}$ ) and  $A_{eff}$  can be calculated by the following equation[50]

$$A_{eff} = \frac{[\int I(r)rdr]^2}{[\int I^2(r)rdr]^2} \quad (4.28)$$

where,  $I(r) = |E_t|^2$  indicates the intensity of the electric field distribution across the cross section area of the fiber. Effective area  $A_{eff}$  of the fiber is used to calculate the nonlinearity of the fiber.

The terms linear and nonlinear, in optics, stand for intensity-independent and intensity dependent phenomena respectively. Non-linear effects in optical fibers occur due to either change in the refractive index of the medium with optical intensity or inelastic-scattering phenomenon. The power dependence of the refractive index is responsible for the Kerr-effect. The nonlinear properties of the PCF greatly depend on the core parameters that determine the effective mode area. The nonlinear properties of a fundamental mode can be measured by the nonlinearity coefficient  $\gamma$  defined as [53]

$$\gamma = \left(\frac{2\pi f}{c}\right) \left(\frac{n_2}{A_{eff}}\right) \quad (4.29)$$

Here,  $n_2$  is kerr coefficient and for Zeonex it is about  $2 \times 10^{-20} [m^2/W]$ .

## 4.5 Conclusion

In this chapter, theories related to our work has been described. Propagation theory and wave equation is described which is the key of numerical solve. Besides, different parameters like effective index, effective material loss, dispersion and birefringence are described which are the main ones for our work.

# Chapter 5

## PROPOSED MODELS AND SIMULATION RESULTS

### 5.1 Introduction

In this chapter, we will discuss about two proposed models and their simulation results. Also, we will plot the parameters like effective index, effective material loss, confinement loss, dispersion and birefringence against various frequency and core length. Finally, we will compare our model with other recently proposed models by various research teams.

### 5.2 Proposed Models

We have designed and simulated two models. In this section, structure of two models will be discussed.

We have used COMSOL 5.0, a finite element based software, for both the design and simulation of the geometrical models of both the proposed PCF. Figure 5.1 shows the cross-sectional view of our proposed model 1. In model 1, the fiber core is rectangular in shape. The core length is defined as  $L_c$  and the width as  $W_c$ . In this proposed model, the core width ( $W_c$ ) is kept 1.1 times the core length ( $L_c$ ) throughout the entire simulation process. The optimum fiber core length ( $L_c$ ) and core width ( $W_c$ ) are selected as 400  $\mu\text{m}$  and 440  $\mu\text{m}$  respectively. The elliptical air-hole in the core is chosen to create greater asymmetry in the core region. Each ellipse in the core has major axis of  $a$  and minor axis of  $b$ . The value of  $a$  and  $b$  are chosen as  $a = 0.47 \times L_c$  and  $b = 0.1 \times L_c$ .  $P_c$  is defined as the core pitch which is the distance between the centers of two adjacent elliptical air-holes.  $P_c$  is set to  $L_c/3$  in the model. Each circular air-hole has a radius of  $L_c/10.5$ . Addition of these circular air-holes with elliptical air-holes in the core region makes the fiber less absorbent, highly birefringent and offers nearly zero flattened dispersion profile.

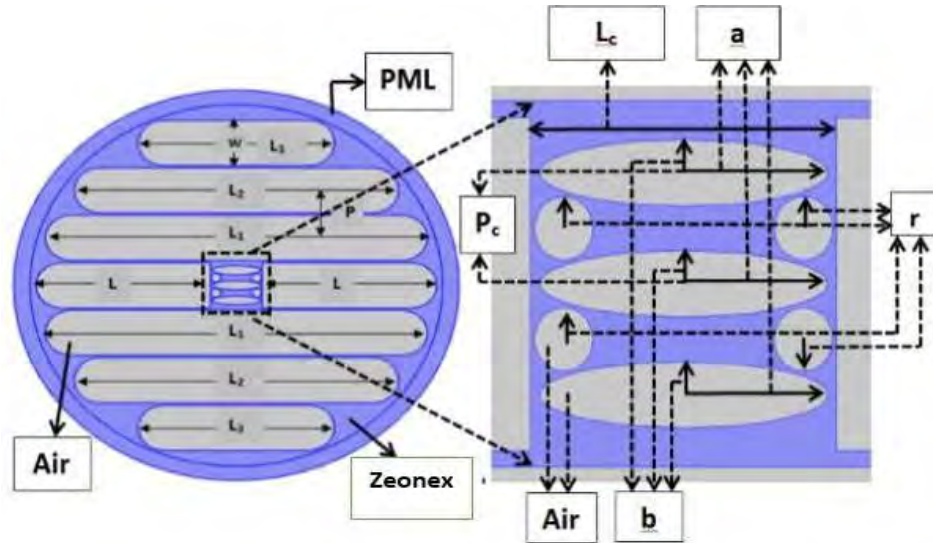


Figure 5.1: Cross Sectional view of the proposed model 1.

Porosity is a term used to define the percentage of area covered by the air-holes in the fiber solid core. At higher core porosity the index difference between core and cladding decreases hence it is difficult to confine the modal power to the core. On the other hand, the effective material loss is higher at lesser core porosity due to the presence of much material in the core region. Hence to make a tradeoff between these two losses, the optimum porosity is taken as 50% throughout the entire simulation period.

In the cladding region in total of eight rectangular slots are used with same width ( $w$ ) as seen from Fig.5.1 with different lengths, however, the number of slots is less than that of a recently proposed model[19]. So, the fabrication will be easier. The upper three slots are mirror of lower three slots. The length of the slots  $L$ ,  $L_1$ ,  $L_2$ ,  $L_3$  are  $2.43 \times L_c$ ,  $7.4 \times L_c$ ,  $6.28 \times L_c$  and  $3.8 \times L_c$  respectively. Each slot in the cladding has width ( $w$ ) equal to  $L_c$ . Cladding pitch defined as  $P$  is set to  $1.05 \times L_c$ . The compact rectangular slots in the cladding help confine higher modal power in the core. These slots also help in trading off the material absorption loss and the confinement loss by permitting the air-holes of larger dimension in the core region. This total scheme reduces the material significantly in the core region and also enhances the contrast of index between core and cladding. Such arrangement also makes the dispersion profile more flat. A perfectly matched layer which is about 8% of the total radius of the fiber is used to truncate computational regions.

The cross section of the proposed model 2 of the PCF with enlarged version of the core is shown in Fig. 5.2. The elliptical core has major axis and minor axis length of  $2a$  and  $2b$  respectively. A horizontally aligned and a vertically aligned strut are used in the following model to support the core inside the fiber firmly. Because of the suspended core, the refractive index of the cladding region may be considered as unity. This scheme helps confine the modal power more tightly inside the core.

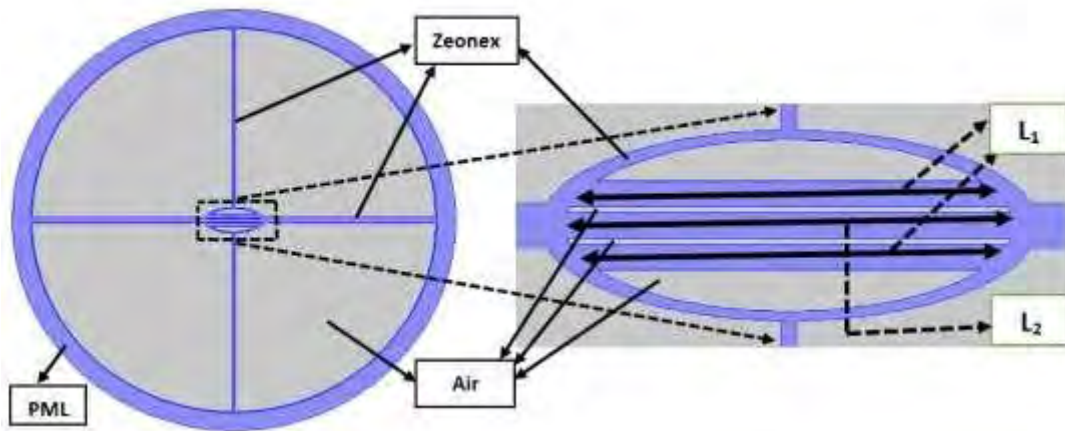


Figure 5.2: Cross section of the proposed model 2.

The horizontally aligned strut is intentionally made larger in dimension than that of vertically aligned strut in order to create asymmetry in the structure. Both the horizontally and vertically aligned struts have thickness of  $0.21a$  and  $0.067a$  respectively. They both have the same length of  $13.33a$ . A set of three strut having same thickness of  $0.12a$  but different length of  $L_1, L_2, L_3$  is used inside the core.  $L_1, L_2, L_3$  are set as  $1.76a, 1.8a$  and  $1.76a$  respectively. The core pitch denoted as  $\Lambda_c$  is the distance between two adjacent struts and it is set as  $0.15a$  for this proposed model. The dimension of the core air-slots inside the core region depends on major axis core length  $2a$ . In this proposed model, the optimum porosity is chosen as 35.1%. The total fiber diameter is chosen as  $13.33a$ . The optimum major axis core length and minor axis core length are selected as  $2a = 440\mu\text{m}$  and  $2b = 195\mu\text{m}$  respectively at core porosity of 35.1% and operating frequency of 1THz.

There are several materials available that can be used to design terahertz waveguides. Such materials include polymethyl-methacrylate (PMMA), High density polyethylene (HDPE), Teflon, Topas etc. which are discussed in chapter 3. Most of the recent simulation and experimental works on THz waveguides have been performed taking Topas as background



material due to its several unique favorable qualities such as low water absorption, low material absorption loss ( $0.2 \text{ cm}^{-1}$ ), much higher glass transition temperature( $T_g$ ) than PMMA, good for bio-sensing. Moreover, its constant refractive index (1.535) over a wide terahertz frequency band makes the chromatic dispersion negligible. However, we choose a latest cyclo-olefin polymer (COP) named as Zeonex as the background material for both of the proposed models because of its unique advantages over Topas including lower content of impurities, higher heat resistance, lower dielectric constant and loss tangent. Moreover, it has lower specific gravity, higher chemical resistance at elevated temperature, higher transparency, lower melt flow index etc. Furthermore, the physical properties of Zeonex are also suitable for high quality fiber drawing compared to Topas. Also, fluctuations in the fiber diameter are reduced because of the greater stability of drawing process. This allows more degrees of freedom in fiber design. In addition, it offers a wide range of drawing stress which makes the fabrication much easier.

### 5.3 Simulation Results

Finite element modeling (FEM) package, COMSOL 5.0, was used to solve Maxwell's equation for both of the proposed models. During simulation of both models, we selected *extremely fine* mesh that divided the whole PCF into a large number of mesh elements that enhance the accuracy of fiber characterization. We found that the total number of elements composing the mesh of both models are 22,214 and 11,794 respectively. The average element quality is 0.90 and 0.87 respectively. Therefore, computational error using COMSOL is nearly 0.1%. To perform such simulations, we solved for the complex effective refractive indices and field profiles of the first  $N=20$  modes for both of the models. During standard fabrication,  $\pm 2\%$  variation of the global diameter of the PCF was taken into consideration for each of the models.

#### 5.3.1 Simulation result of proposed model 1

Figure 5.3 shows the modal power flow distribution in the fiber for both x and y polarization modes for model 1. For the porous core fibers, the effective refractive index of the both core and cladding is reduced because of the introduction of air-holes in both regions. These air-holes in core region are introduced in order to reduce the material absorption loss and in cladding region to reduce the confinement loss. A part of the total modal power penetrates

through the cladding region due to some loosely bounded modes in the fiber core region as observed in Fig. 5.3.

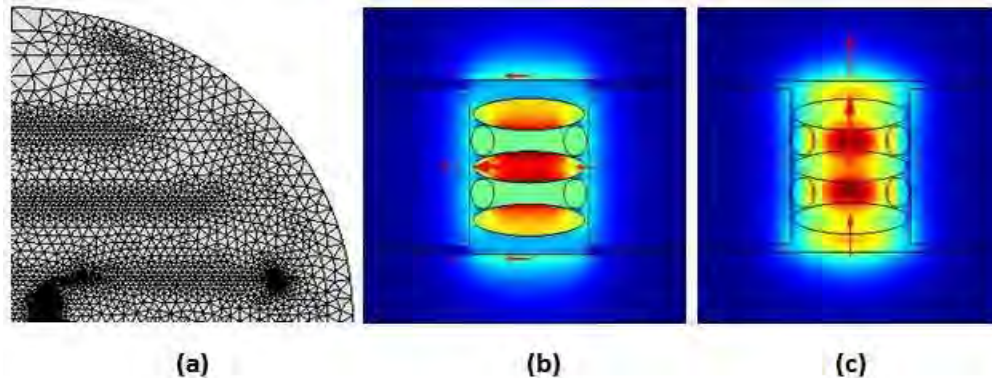


Figure 5.3: (a) Mesh of the proposed PCF (model 1); Mode field distribution at  $L_c = 400\mu\text{m}$  and  $f = 1\text{ THz}$  for (b) x-polarization mode; and (c) y-polarization mode.

First, effective refractive index for both x and y polarization modes is plotted against various core length ( $L_c$ ) and frequency ( $f$ ) as shown in Fig. 5.4 and Fig. 5.5 respectively. It is observed that effective index increases with the increase in core length and frequency as well. It is obvious that with the increase in core length, the material in the core region is increased and this results in higher effective refractive index. As the refractive index is a function of frequency, it is also increased with the increase in frequency. However, increase in material in core causes higher effective material loss. At optimum core length of  $400\mu\text{m}$ , core porosity of 50% and operating frequency of  $1\text{ THz}$ , the refractive index for x and y-polarization mode are 1.124 and 1.206 respectively.

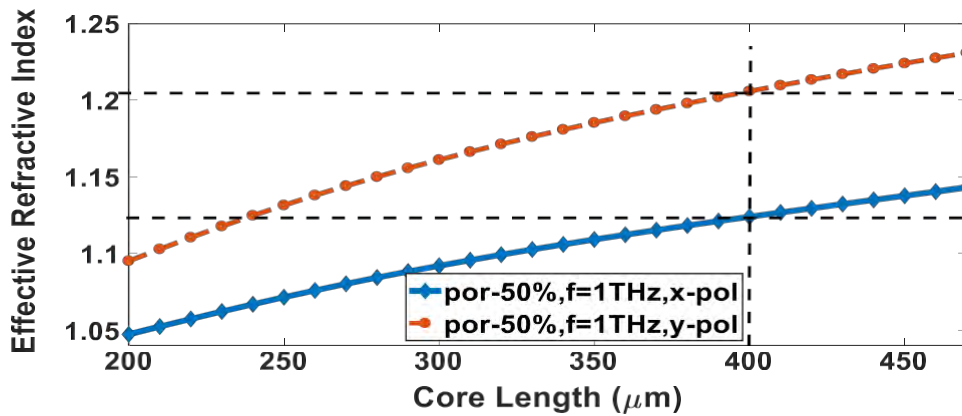


Fig. 5.4: Effective refractive index as a function of core length at  $f=1\text{ THz}$  for model 1.

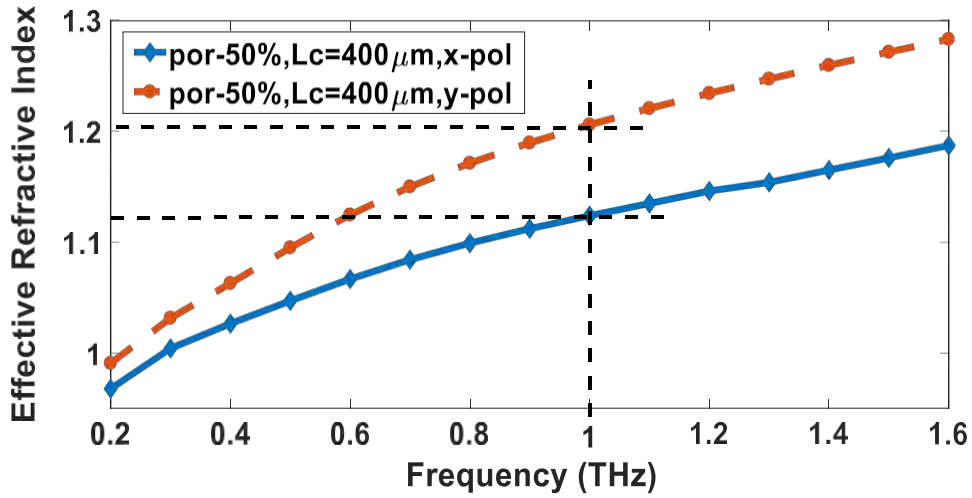


Fig. 5.5: Effective refractive index as a function of frequency at  $L_c = 400\mu\text{m}$  for model 1.

Normalized frequency or  $V$ -parameter is computed to ensure whether the fiber operates at single-mode or multi-mode by the following equation

$$V = \frac{2\pi r f}{c} \sqrt{(n_{co}^2 - n_{cl}^2)} \leq 2.405, \quad (5.1)$$

where,  $r$  is the radius of the core,  $f$  is the operating frequency,  $c$  is the speed of the light in free space,  $n_{co}$  and  $n_{cl}$  are the refractive indices of the fiber core and cladding respectively.  $n_{cl}$  is considered to be nearly 1. It is due to the fact that, cladding is mainly consisted of compact rectangular air-holes and  $n_{co}$  is considered to be  $n_{eff}$  because core has material and air holes. In order to maintain single mode operation, the value of  $V$ -parameter must be equal to or less than 2.405.

$V$ -parameter as a function of core length ( $L_c$ ) and frequency ( $f$ ) are shown in Fig. 5.6 and Fig. 5.7 respectively. It is seen from both the figures that the single mode operating condition is maintained when  $L_c < 430 \mu\text{m}$  and  $f < 1.1 \text{ THz}$  for x-polarization mode and for the y-polarization mode it is maintained when  $L_c < 360 \mu\text{m}$  and  $f < 0.9 \text{ THz}$ . Keeping this in mind, the operating frequency and core length are kept within the single mode limit for x-polarization mode.

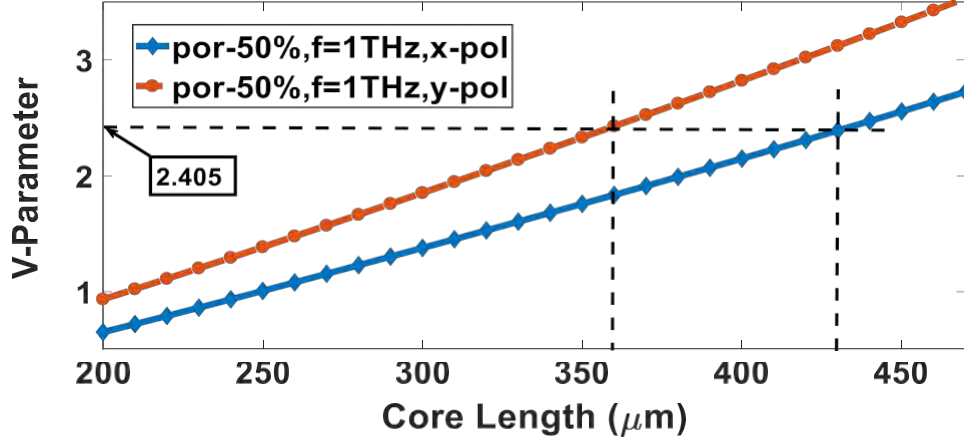


Fig. 5.6:  $V$ -parameter as a function core length at  $f=1$  THz for model 1.

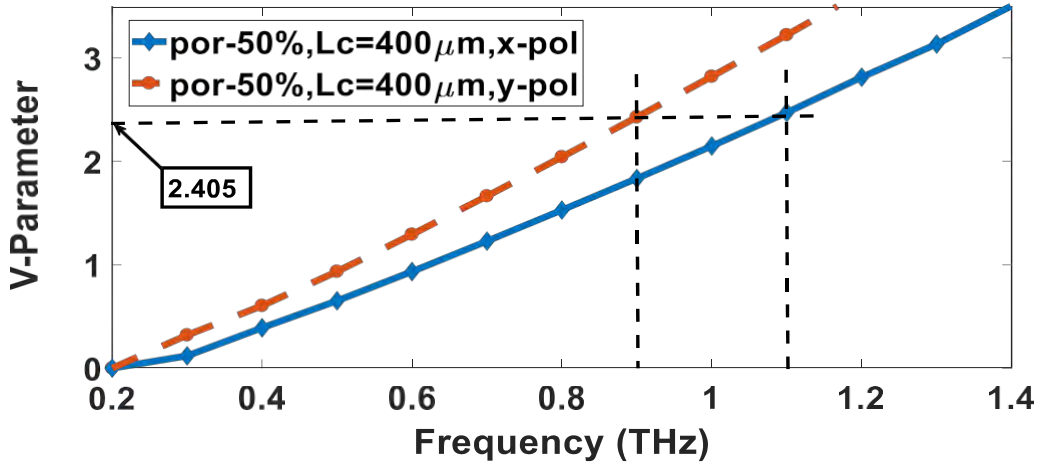


Fig.5.7:  $V$ -parameter as a function of frequency at  $L_c=400\mu\text{m}$  for model 1.

The major loss component of the fiber is the material absorption loss or effective material loss (EML) which can be calculated by the following formula

$$\alpha_{\text{eff}} = \sqrt{\frac{\epsilon_0}{\mu_0}} \left( \frac{\int_{\text{mat}} n_{\text{mat}} |E|^2 \alpha_{\text{mat}} dA}{|\int_{\text{all}} S_z dA|} \right), \text{ cm}^{-1} \quad (5.2)$$

where  $\alpha_{\text{mat}}$  is the material absorption loss,  $n_{\text{mat}}$  is the refractive index of the background material,  $\alpha_{\text{mode}}$  is the fundamental mode loss,  $E$  is the modal electric field,  $S_z$  is the z-component of the pointing vector ( $S_z = \frac{1}{2} (\mathbf{E} \times \mathbf{H}^*) \cdot \hat{z}$ ) and  $\epsilon_0$  and  $\mu_0$  are the permittivity and permeability of free space, respectively. The effective material loss mainly depends on the amount of solid background material used in the fiber. The absorption loss is maximum when

only solid material is used. Introduction of air hole of appropriate porosity in the core reduces the material loss to a great extent.

Effective material loss (EML) as a function of core length ( $L_c$ ) and frequency ( $f$ ) are shown in the Fig. 5.8 and Fig. 5.9 respectively. From both the figures, we see that EML increases with the increase in  $L_c$  and  $f$  for both x and y polarization modes. It is because at higher core length the solid material in the core region is increased, as a result, EML is increased. According to the empirical formula  $\alpha(v) = v^2 + 0.63v - 0.13$ ,  $\text{cm}^{-1}$ [64], where  $v$  stands for frequency, we can also conclude that, EML is increased with the increase in frequency. It is because of the porous core fiber, which confines more and more of the light into the solid material between the holes as the frequency gets higher. Although at smaller core length and lower frequency, EML is much lower for x polarization mode, we have picked  $L_c = 400 \mu\text{m}$  as optimal core length and  $f = 1 \text{ THz}$  as optimal operating frequency. Because at  $L_c = 400 \mu\text{m}$  and  $f = 1 \text{ THz}$ , the confinement loss is very low, birefringence and modal power flowing through core air-hole are higher and effective area for the fiber is also greater for both degenerative modes. Between these two orthogonal modes, only x-polarization mode will be taken into consideration throughout whole simulation process since better results are obtained for it. At optimum core length, core porosity and operating frequency, the effective material loss for x polarization mode is only  $0.0448 \text{ cm}^{-1}$ . This obtained value is obviously less than that of the works previously reported.

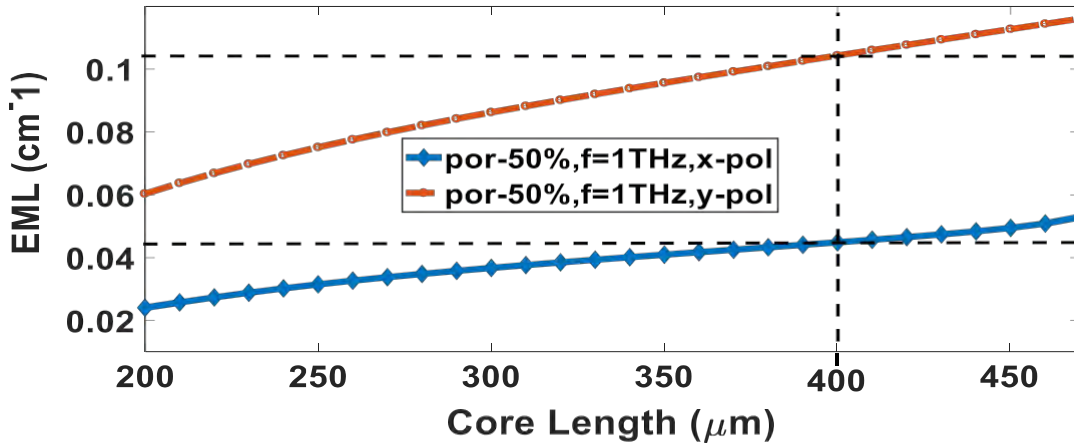


Fig. 5.8. EML as a function of core length at  $f = 1 \text{ THz}$  for model 1.

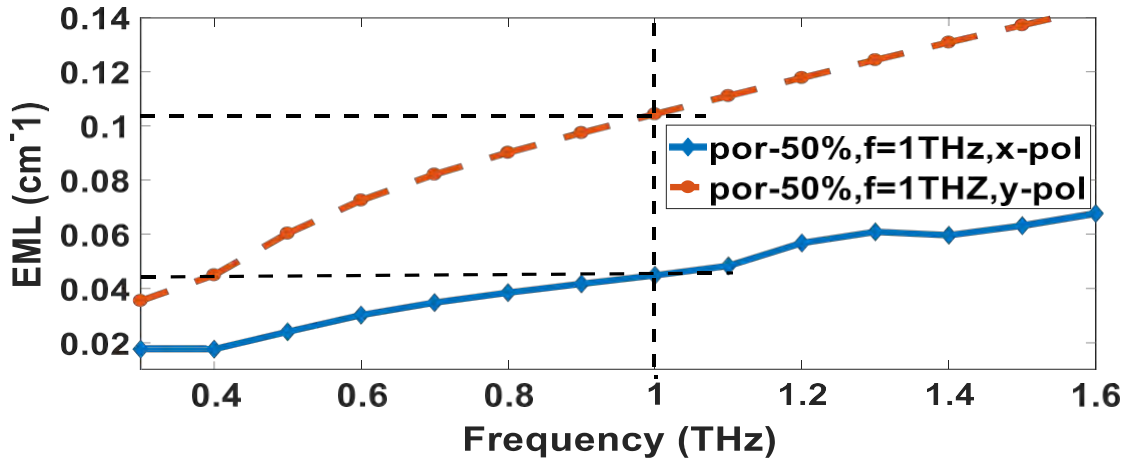


Fig. 5.9. EML as a function of frequency at  $L_c = 400\mu\text{m}$  for model 1.

Birefringence is another important parameter that determines whether the fiber can be used in polarization maintaining applications. There are basically two key methods for making a PCF highly birefringent. It can be done either by breaking the symmetry of the geometry of the core or creating asymmetry in the cladding region. The greater asymmetry is desirable to achieve higher birefringence. This parameter can be calculated by the following equation

$$B = |n_x - n_y| \quad (5.3)$$

where,  $B$  represents the phase birefringence,  $n_x$  and  $n_y$  represent refractive indices of orthogonal polarization modes. It is also known as modal birefringence. Both fig. 5.10 and fig. 5.11 show the variation of phase birefringence for various core length ( $L_c$ ) and frequency ( $f$ ). It is seen from the both figures that with the increase in core length and frequency, there is an increase in phase birefringence for particular core porosity. It is due to the fact that material in the core region is increased with larger core length. The increase in material causes more confinement of field in the core and more asymmetry. Eventually it increases the effective refractive index difference between x and y polarization modes. However, EML is higher at larger core length and increases with frequency. So we cannot choose larger core length and higher frequency for higher birefringence. At optimum core length, frequency and core porosity, the phase birefringence is 0.0818. This result is higher than that of the previously reported works.

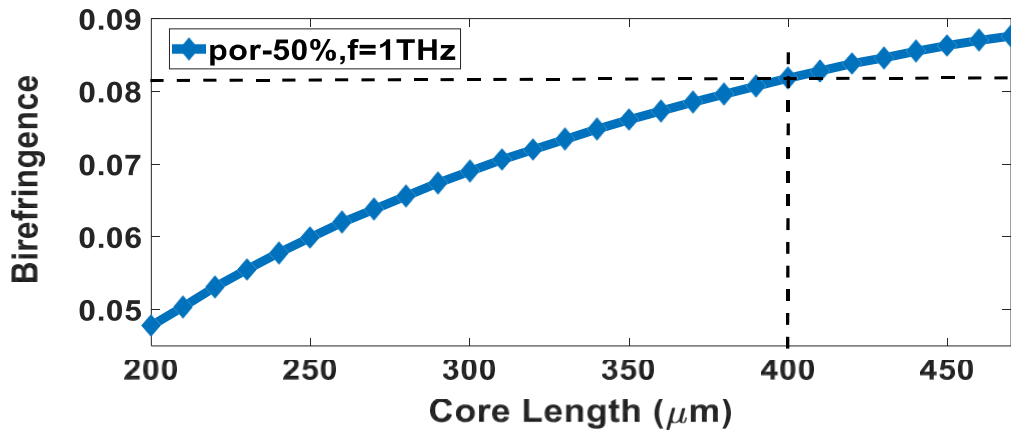


Fig.5.10: Phase birefringence as a function core length at  $f=1\text{THz}$  for model 1.

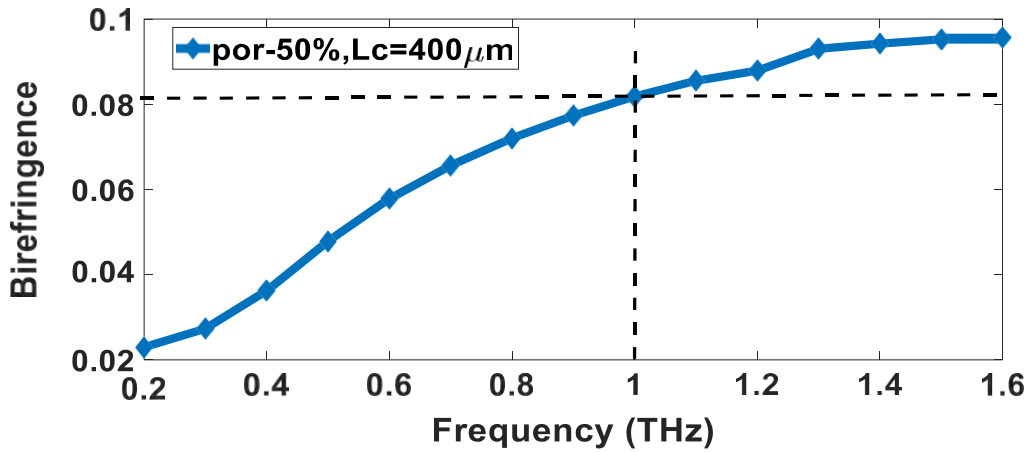


Fig.5.11: Phase birefringence as a function of frequency at  $L_c = 400\mu\text{m}$  for model 1

Once modal birefringence is known, group birefringence can also be calculated by using the formula given bellow

$$G_B = B - \lambda \frac{dB}{d\lambda}, \quad (5.4)$$

where,  $G_B$  is the group birefringence and ' $\lambda$ ' be the wavelength. Group Birefringence for various frequency is plotted and shown in figure 5.12. It is seen that group birefringence decreases with the increase in frequency.

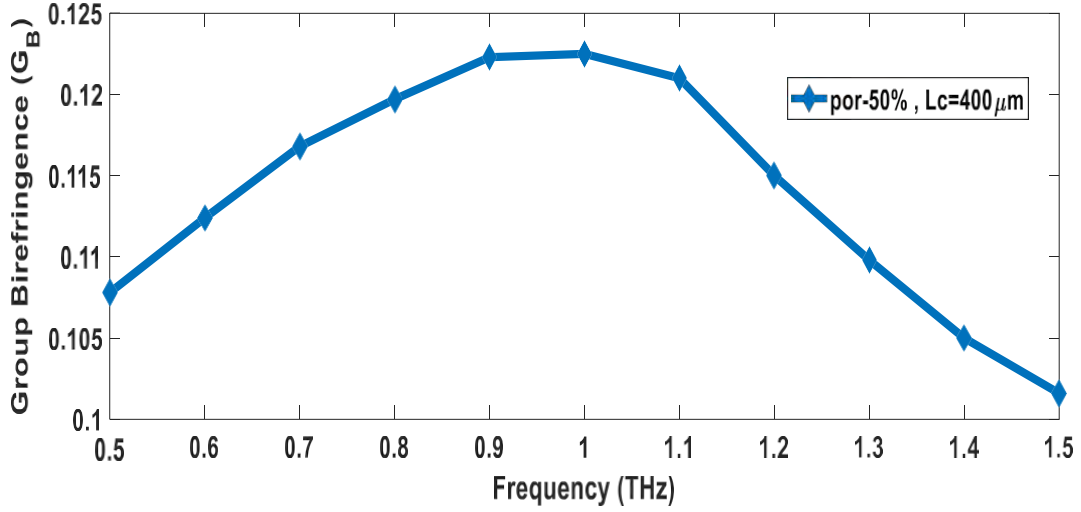


Fig.5.12: Group birefringence as a function of frequency at  $L_c = 400\mu\text{m}$  for model 1

An important linear characteristic that limits the bandwidth or information carrying capacity of the fiber is dispersion. Dispersion is the spreading of light pulse as it travels along the length of a fiber. Modal, material and waveguide dispersion are three types of the dispersion that may occur in a fiber. Modal dispersion occurs only in multimode fibers and material dispersion occurs due to the dependency of the refractive index of material on frequency. As our fiber is Zeonex based single mode fiber, so the modal and material dispersion are almost zero. Hence, only waveguide dispersion is to be calculated for the proposed waveguide. The waveguide dispersion depends on the structure of the waveguide itself and can be calculated by

$$\beta_2 = \frac{2}{c} \frac{dn_{eff}}{d\omega} + \frac{\omega}{c} \frac{d^2 n_{eff}}{d\omega^2}, \text{ ps/THz/cm} \quad (5.5)$$

where,  $\omega = 2\pi f$ ,  $c$  is the velocity of light in vacuum and  $n_{eff}$  is the effective refractive index of the fiber. Figure 11 shows the variation of dispersion for x and y polarization modes as a function of frequency. From the Fig. 5.12, it is seen that, at optimum core length and core porosity, between two modes, dispersion for x-polarization mode is lower and more flat than that of previously reported works. It is about  $1.196 \pm 0.08$  ps/THz/cm and remains flat within 0.9-1.6 THz.



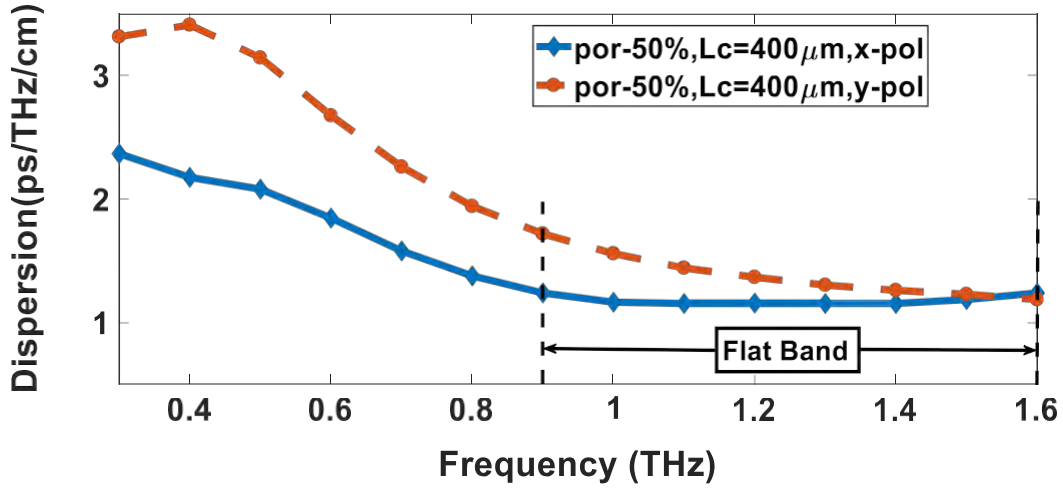


Fig.5.13: Dispersion as a function of frequency at  $L_c = 400\mu\text{m}$  for model 1

Another important parameter that determines the performance of the porous-core fiber is the confinement loss. This loss component occurs due to the finite number of air-hole rings used in the cladding and limits the terahertz signal transmission. This loss can be computed by the following equation

$$L_{con} = \left( \frac{4\pi f}{c} \text{Im}(n_{eff}) \right), \text{cm}^{-1} \quad (5.6)$$

Where,  $L_{con}$ ,  $f$  and  $c$  are defined as the confinement loss, frequency and speed of the light respectively and  $\text{Im}(n_{eff})$  represents the imaginary part of the complex effective refractive index.

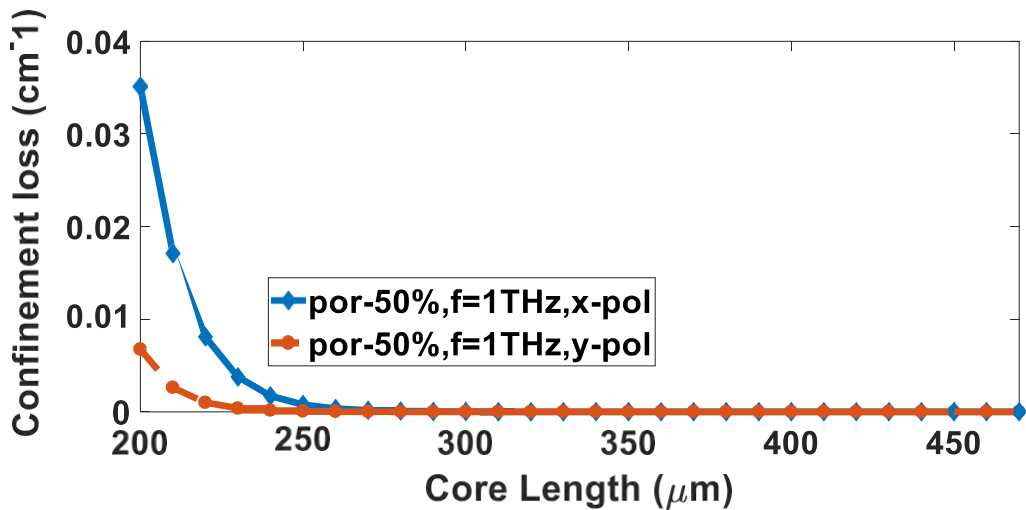


Fig.5.14 : Confinement loss as a function of core length at  $f=1\text{THz}$  for model 1

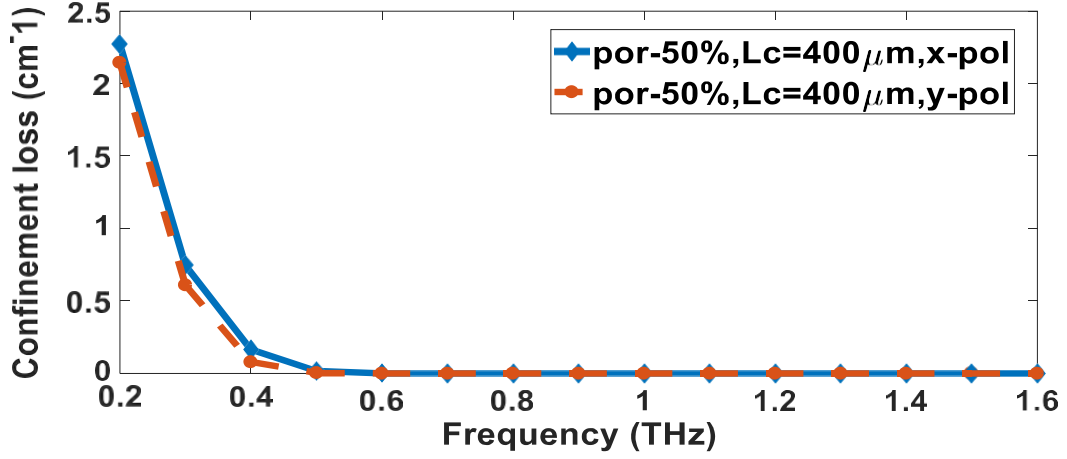


Fig.5.15 : Confinement loss as a function of frequency at  $L_c=400\mu\text{m}$  for model 1

From Fig. 5.13 and Fig. 5.14, we can see that, for both x and y polarization modes, the confinement loss decreases with the increase in core length and frequency for a particular core porosity. It is due to the fact that, at higher core length and frequency, the refractive index difference between core and cladding increases and hence the modal power is forced to be propagated through the core. This loss component can also be minimized either by increasing the number of air-holes or porosity of the cladding. At optimum core length, operating frequency and core porosity, the value of the confinement loss for both orthogonal polarization mode is negligible compared to effective material loss and it is about  $3.99 \times 10^{-7} \text{ cm}^{-1}$  for x-polarization mode and  $1.81 \times 10^{-9} \text{ cm}^{-1}$  for y polarization mode respectively. Since for x-polarization mode, the fiber loss and dispersion characteristic are better than that of y-polarization mode at optimum operating condition, confinement loss of x-polarization mode is taken into consideration.

It is much desirable to flow the power through the core air holes of fiber since dry air does not absorb terahertz power. The power fraction ( $\eta$ ) is calculated to determine the amount of power propagated through fiber's different regions. The core power fraction ( $\eta_c$ ) is defined as the fraction of total modal power flowing through the core air holes of the fiber. It can be calculated by the following formula

$$\eta_c = \frac{\int_{\text{core air holes}} S_z dA}{\int_{\text{all}} S_z dA}, \quad (5.7)$$

where, the integration in the numerator is over the region of core air holes and the integration in the denominator is over the total fiber region. Figure 5.15 and 5.16 show the variation of core power fraction for various core length ( $L_c$ ) and frequency ( $f$ ) respectively. It is seen that, at larger core length and frequency, the percentage of the modal power in the core air-holes for both orthogonal polarization mode is increased. At optimum core length, frequency and core porosity, for x polarization mode, it is nearly 55.3% and much higher than that of previously reported works.

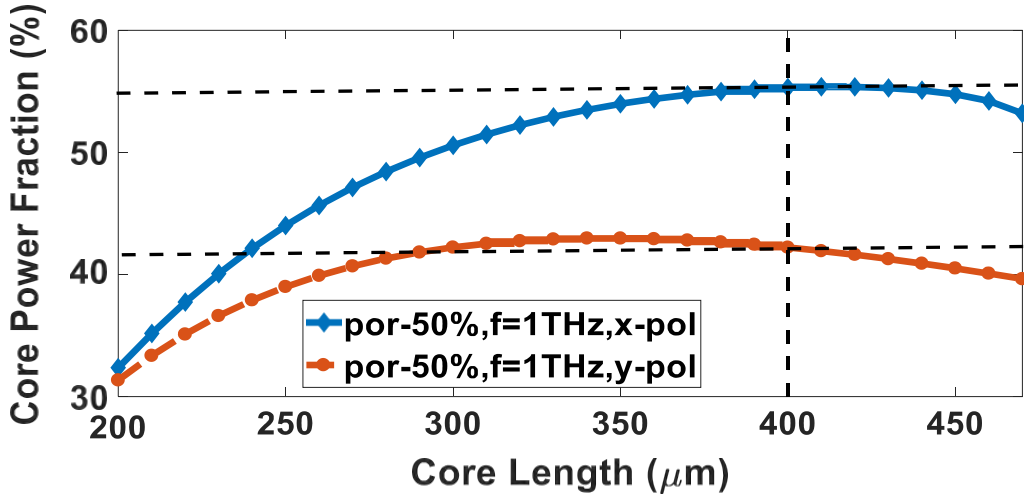


Fig.5.16: Core power fraction as a function of core length at  $f = 1$  THz for model 1

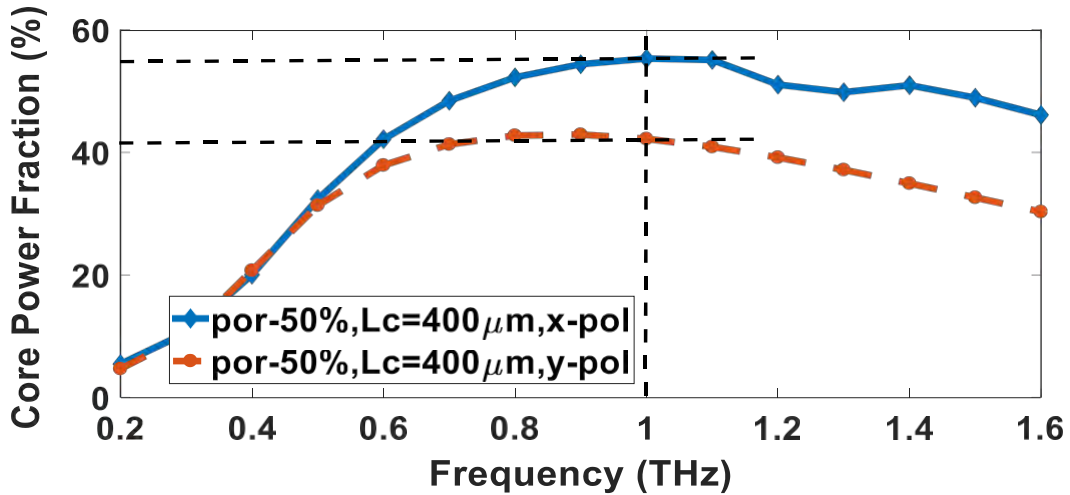


Fig.5.17: Core power fraction as a function of frequency at  $L_c = 400 \mu\text{m}$  for model 1

The area covered by electromagnetic waves in the core region is called effective area ( $A_{eff}$ ) and  $A_{eff}$  can be calculated by the following equation

$$A_{eff} = \frac{[\int I(r)rdr]^2}{[\int I^2(r)rdr]^2}, \quad (5.8)$$

where,  $I(r) = |E_t|^2$  indicates the intensity of the electric field distribution across the cross section area of the fiber. Effective area  $A_{eff}$  of the fiber is used to calculate the nonlinearity of the fiber. At optimum core length, frequency and core porosity, it is seen from the fig. 5.17 and fig. 5.18, effective area of the fiber is about  $1.32 \times 10^5 \mu m^2$  for x-polarization mode and it is about  $1.29 \times 10^5 \mu m^2$  for y-polarization mode.

The terms linear and nonlinear, in optics, stand for intensity-independent and intensity dependent phenomena respectively. Non-linear effects in optical fibers occur due to either change in the refractive index of the medium with optical intensity or inelastic-scattering phenomenon. The power dependence of the refractive index is responsible for the Kerr-effect. The nonlinear properties of the PCF greatly depend on the core parameters that determine the effective mode area. The nonlinear properties of a fundamental mode can be measured by the nonlinearity coefficient  $\gamma$  defined as

$$\gamma = \left(\frac{2\pi f}{c}\right) \left(\frac{n_2}{A_{eff}}\right), \quad (5.9)$$

Here,  $n_2$  is kerr coefficient and for Zeonex it is about  $2 \times 10^{-20} [m^2/W]$ . Nonlinearity  $\gamma$  of the fiber as a function of frequency at  $L_c=400\mu m$  is shown in fig.5.19. It is seen from the figure that it increases with the increase in frequency. Fiber nonlinearity is inversely proportional to the effective area ( $A_{eff}$ ) of the fiber. For long distance transmission of terahertz waves, lower nonlinearity is expected. As the effective area of the fiber for x-polarization mode is greater than that of y-polarization mode, it shows negligible nonlinearity. At optimum operating parameters, it is only  $3.33 \times 10^{-9} W^{-1}m^{-1}$ .

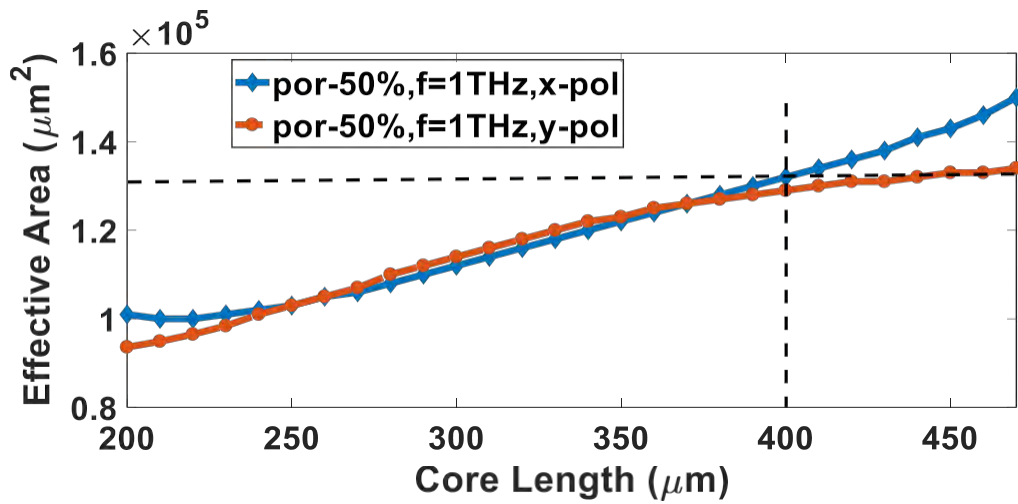


Fig.5.18: Effective area of the fiber as a function of core length at  $f=1$  THz for model 1

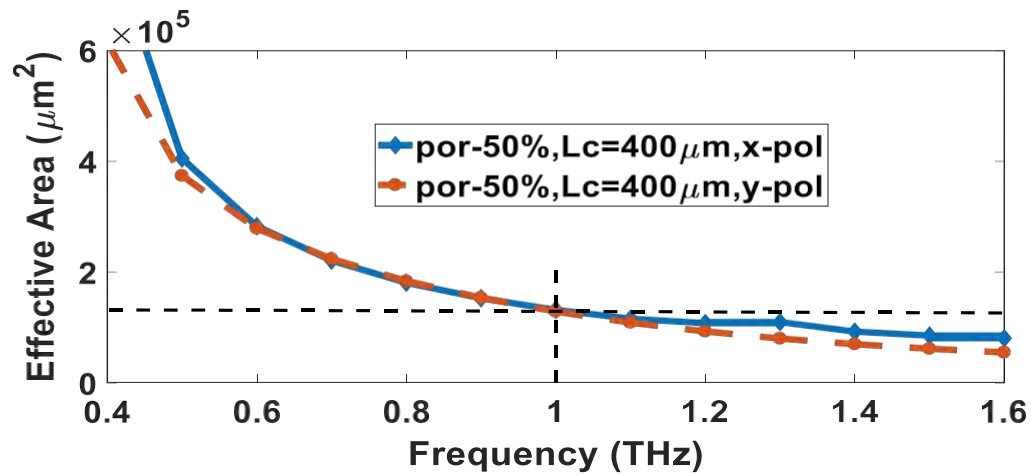


Fig.5.19: Effective area of the fiber as a function of frequency at  $L_c=400\mu\text{m}$  for model 1.

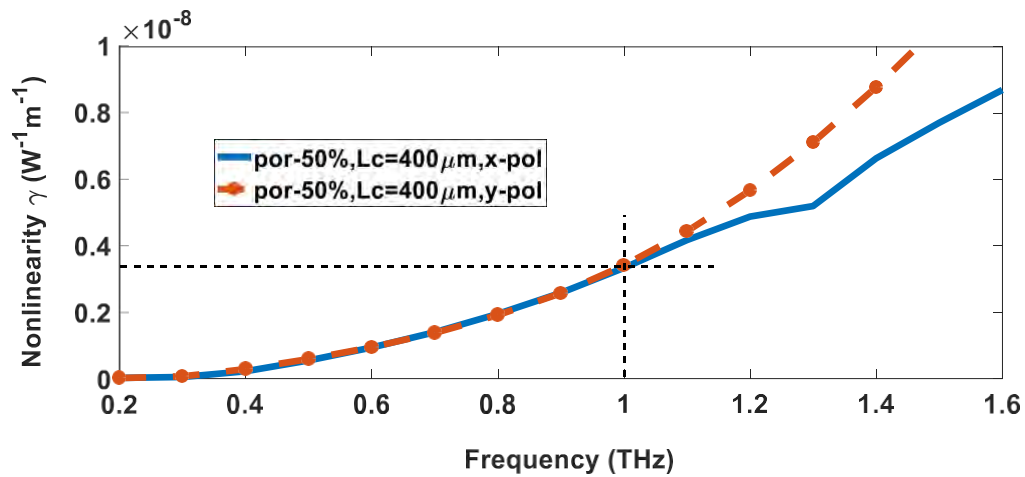


Fig.5.20: Nonlinearity  $\gamma$  of the fiber as a function of frequency at  $L_c=400\mu\text{m}$  for model 1.

### 5.3.2 Simulation result of proposed model 2

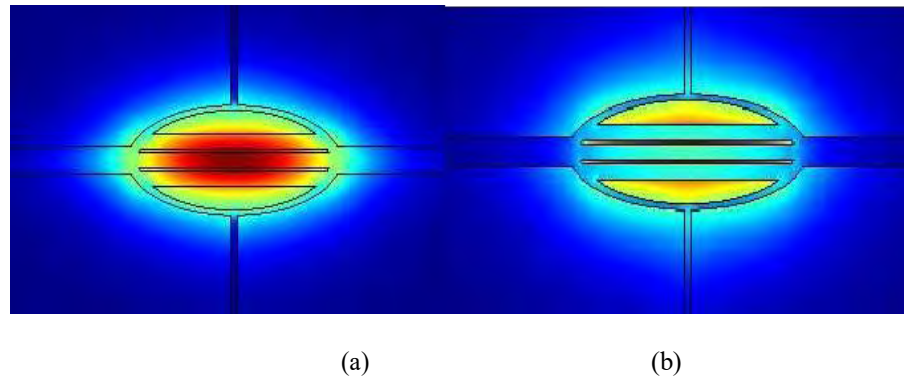


Figure 5.21: Mode power distribution for model 2 (a) x-polarized mode (b) y-polarized mode

Mode power distribution for model 2 at optimum operating parameters is shown for both orthogonal polarized mode in fig. 5.20. Figure 5.20 shows the tight confinement of modal power inside the fiber core for x-polarized mode compared to y-polarized mode. It is due to the fact that, horizontally aligned slots inside the elliptical core create asymmetry by inducing higher index contrast difference between two orthogonal polarized mode in the core region and force the modal power to be confined more tightly for x-polarized mode. Thus, it results low confinement loss for the x-polarized mode. However, material absorption loss is contradictory. As we focus on the material absorption loss and it is low for y-polarized mode with negligible confinement loss, we only take y-polarized mode into consideration throughout the whole simulation period. Some light is seen in the cladding region from the modal power flow distribution in fig. 5.20. Therefore, it can be assumed that, there might be other modes present in the fiber along with single mode but for the other modes light will be propagated through the fiber cladding region. So, when a pulse of light emerges at the center of the fiber only the fundamental mode will be propagated through the core region. The light guiding mechanism in such PCFs is modified total internal reflection (MTIR).

First, effective refractive index at various core porosity for both x and y polarized mode is plotted against various frequency ( $f$ ) and and shown in fig. 5.21. It is seen from the figure that, effective index is higher for x-polarized mode than that of y-polarized mode and it increases for the both orthogonal mode with the increase in frequency. This is because with the increase in frequency more light starts to interact with the material in the core and thus increases the effective refractive index. At higher core porosity the amount of the material in

the core decreases. As a result, the effective refractive index of both orthogonal polarized mode also decreases which results a lower value of birefringence. As our thesis goal is to enhance fiber birefringence, we choose lower porosity. At 35.1% porosity, optimum major axis core length and operating frequency, effective refractive index of the both x and y-polarized mode are 1.2367 and 1.1251 respectively.

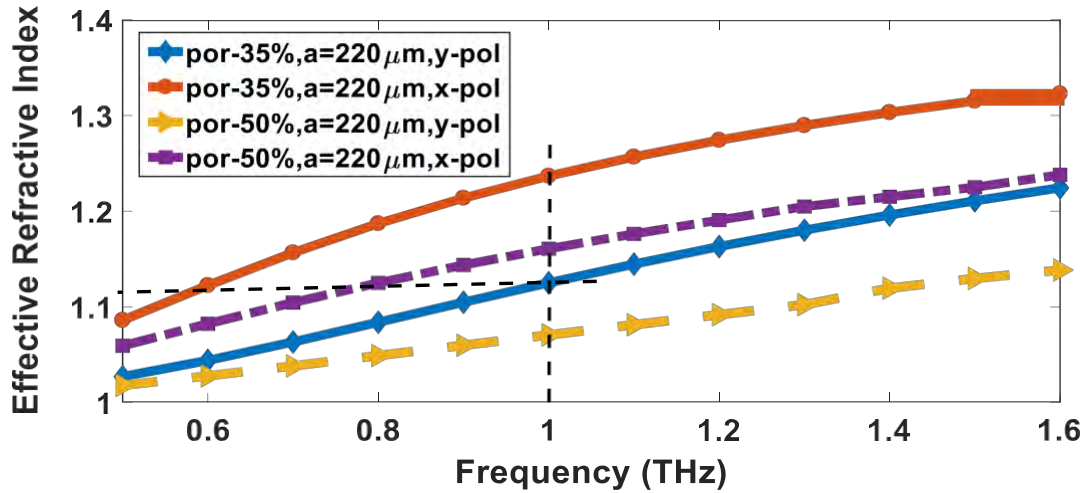


Figure 5.22: Effective refractive index as a function of frequency at  $2a=440\mu\text{m}$  for model 2

For polarization maintaining applications, the fiber has to be highly birefringent. Modal birefringence of a fiber is the difference of the refractive indices between two orthogonal polarized mode and it can be calculated by equation (5.3).

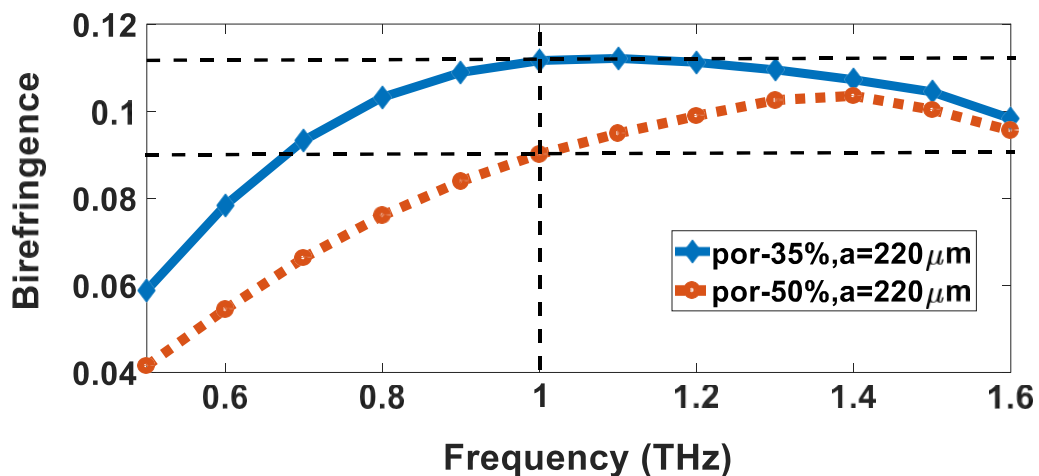


Figure 5.23: Phase birefringence as a function of frequency at  $2a=440\mu\text{m}$  for model 2

Figure 5.22 shows the increase in phase birefringence with the increase in frequency at two different porosities. At lower porosity, the higher amount of the material results higher birefringence. However, lower porosity causes higher material loss in the fiber. Hence, it is a common practice to make a trade-off between birefringence and EML. To do so effectively, we choose  $440\mu\text{m}$  as optimum major axis core length, 35.1% as optimum core porosity and 1THz as optimum operating frequency. At optimum parameters, birefringence for the proposed PCF is 0.1116 and it is the highest anyone ever reported so far for a porous core fiber. Group birefringence is also calculated by equation (5.4) and plotted against various frequency shown in the figure 5.24.

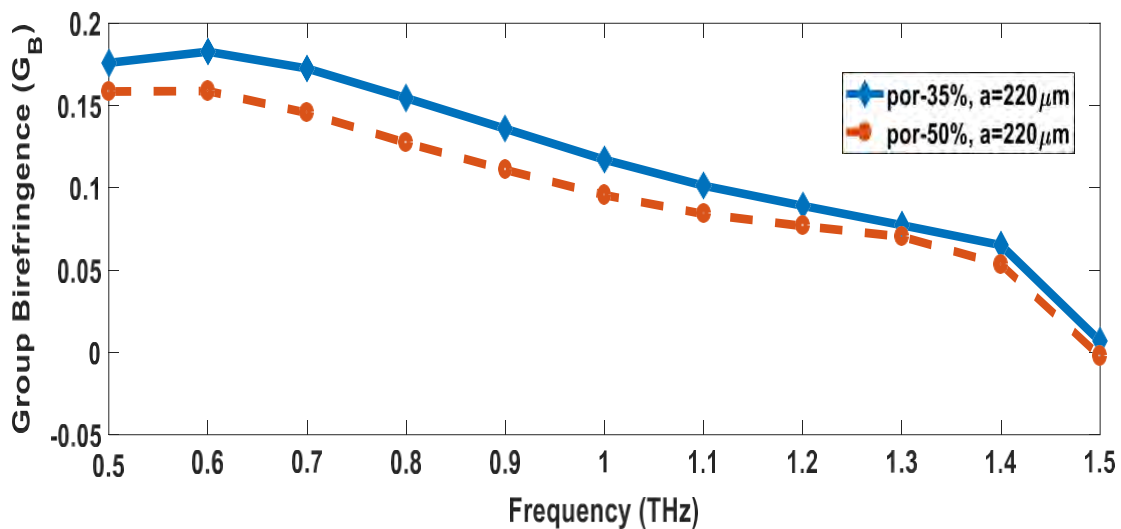


Fig.5.24: Group birefringence as a function of frequency at  $2a = 440\mu\text{m}$  for model 2

Besides, birefringence, it is important to discuss about the loss properties of the PCF. EML and confinement loss are two major loss components. The prime loss mechanism, EML, can be calculated by the equation (5.2). The effective material loss mainly depends on the amount of solid background material used in the fiber. The absorption loss is maximum when only solid material is used. Introduction of air hole of appropriate porosity in the core reduces the material loss.



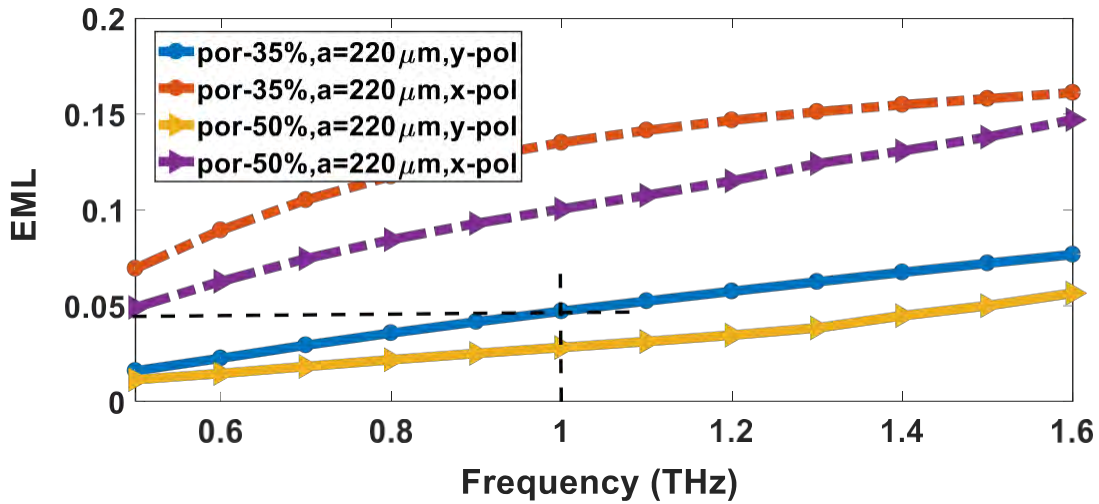


Figure 5.25: EML as a function of frequency at  $2a=400\mu\text{m}$  for model 2

EML as a function of frequency is shown in fig.5.23. It is seen from the figure that, with the increase in frequency, EML increases according to the empirical formulae  $\alpha(\nu) = \nu^2 + 0.63\nu - 0.13$ ,  $\text{cm}^{-1}$ [64], where  $\nu$  stands for frequency. At higher porosity EML is lower. This is because the amount of the material at higher core porosity is lower in the core region which causes lower material loss. However, Birefringence is lower at higher porosity. Hence we make a trade-off. At optimum operating parameters the EML for y-polarized mode is  $0.04716 \text{ cm}^{-1}$  which is better than previously reported works.

Another loss mechanism that determines the length of signal transmission in a terahertz optical waveguide is the confinement loss. It basically depends on the geometrical structure of the waveguide. This loss mechanism can be estimated by equation (5.6).

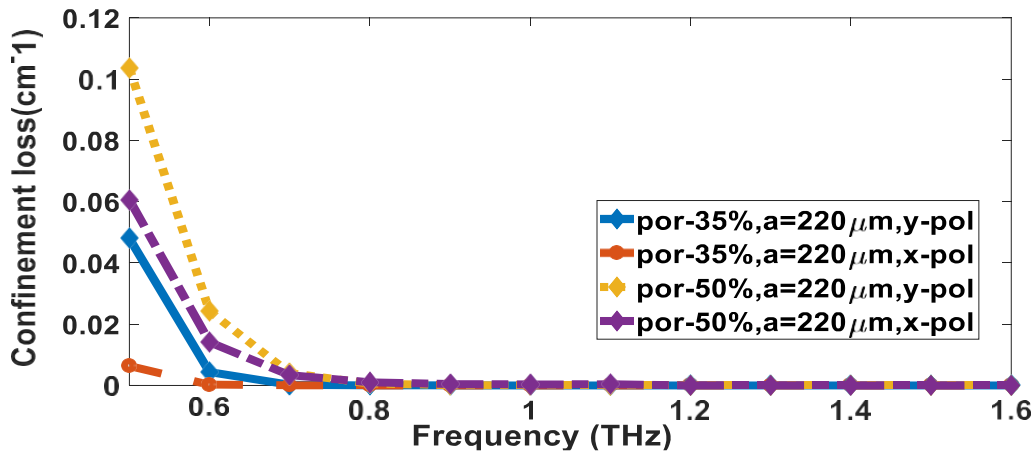


Figure 5.26 : Confinement loss as a function of frequency at  $2a=440\mu\text{m}$  for model 2

Confinement loss as a function of frequency for both polarized mode at different porosity is shown in fig.5.24. It is seen that at different porosity it decreases with the increase in frequency. This is because more light starts to constrict strictly in the porous core region at higher frequency. However, EML is higher at higher frequency. Thus, we select 1 THz as the optimum operating frequency. At 35.1% porosity and at optimum major axis core length and optimum operating frequency, confinement loss for y-polarized mode is  $2.65 \times 10^{-7} \text{ cm}^{-1}$  which is less than that of previously proposed waveguides. Comparing this loss with EML for the same operating parameters we can conclude that confinement loss found for the proposed waveguide is negligible compared to EML which is only  $0.04716 \text{ cm}^{-1}$ .

An important linear characteristic that limits the bandwidth or information carrying capacity of the PCF is dispersion. Dispersion is the spreading of light pulse as it travels along the length of a fiber. Modal dispersion originates only in multimode fibers and material dispersion occurs due to the dependency of the refractive index on frequency. As our fiber is Zeonex based single mode fiber, so the modal and material dispersion is almost zero. Hence, only waveguide dispersion has to be calculated for our PCF. The waveguide dispersion depends on the structure of the waveguide itself and can be calculated by equation (5.5). From the figure it is seen that, dispersion is more flat and lower for y-polarization mode than that of previously reported and it is about  $1.65 \pm 0.45 \text{ ps/THz/cm}$  and remains flat within 1-1.8 THz.

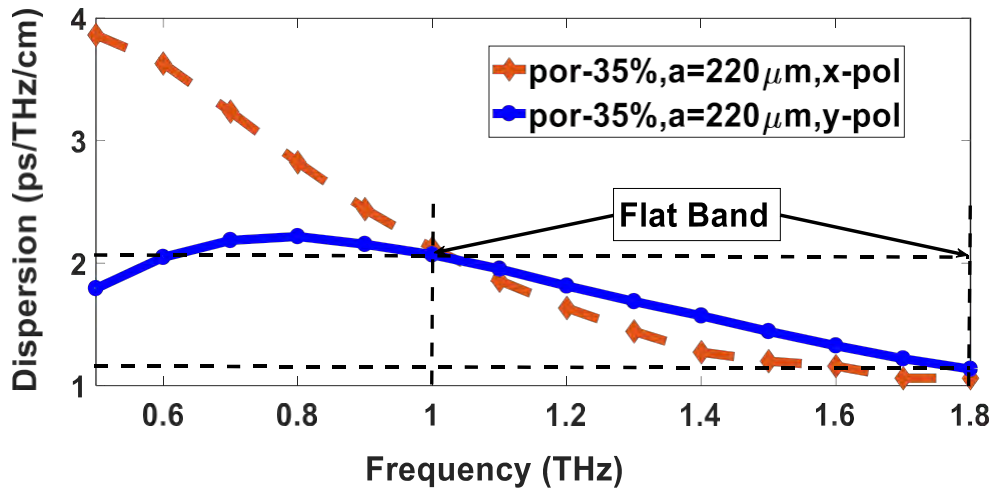


Figure 5.27: Dispersion as a function of frequency at  $2a=440\mu\text{m}$  for model 2

The amount of the power propagating inside the different portion of the fiber can be defined by a term called power fraction. This term can be calculated by equation (5.7). Figure 5.26 shows air core power fraction as a function of frequency at optimum major axis core length. It is seen that at lower porosity the air core power fraction is higher. It is also seen that air core power fraction for y-polarized mode is greater than that of x-polarized mode and it increases with frequency.

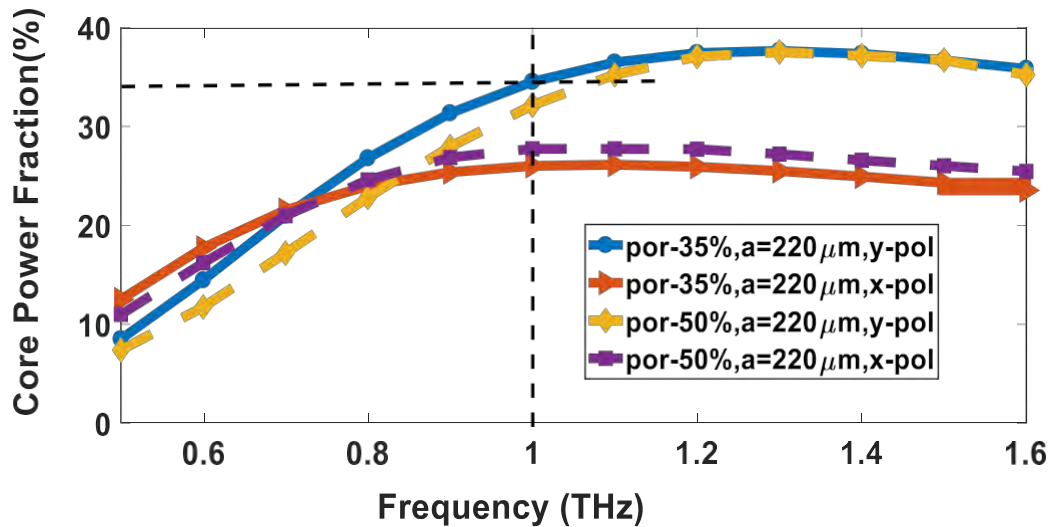


Figure 5.28: Air core power fraction as a function of frequency at  $2a=440\mu\text{m}$  for model 2

It is because with the increase in frequency more modal power is forced to flow inside the air core region. At optimum core porosity, major axis core length and frequency, the air core power fraction for y-polarized mode is about 35%.

Non-linear effects originate from the third-order susceptibility  $\chi^3$ , which is responsible for phenomena such as third-harmonic generation, four-wave mixing (FWM), and nonlinear refraction. This nonlinearity can degrade system performance in some cases while in other situations they might provide a useful application. For long distance transmission of terahertz waves, low non-linearity is expected. This non-linearity is inversely proportional to fiber effective area. The area covered by electromagnetic waves in the core region is called effective area ( $A_{eff}$ ) and it can be estimated by the following equation (5.8). Figure 5.27 shows the variation of fiber effective area with frequency. At optimum parameters, it is seen from the figure 5.27 that, the proposed PCF has an effective area of  $1.24 \times 10^5 \mu\text{m}^2$  for y-polarized mode and it is about  $7.13 \times 10^4 \mu\text{m}^2$  for x-polarized mode. As the effective area of

the fiber for y-polarized mode is greater than that of x-polarized mode thus it shows less non-linearity which is seen in figure 5.28. This parameter can be calculated by equation (5.9).

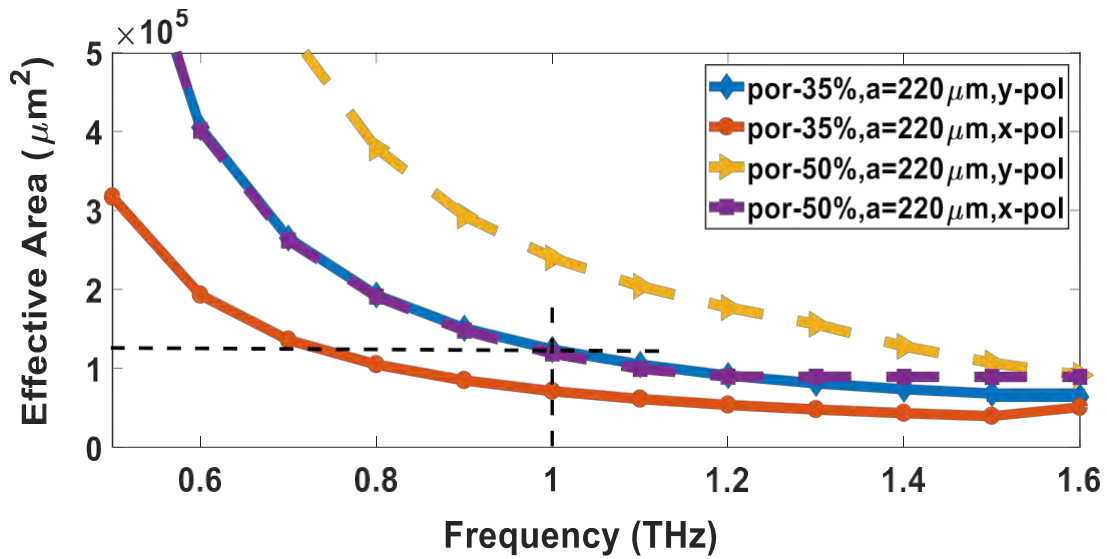


Figure 5.29: Effective area of the fiber as a function of frequency at  $2a=440\mu\text{m}$  for model 2

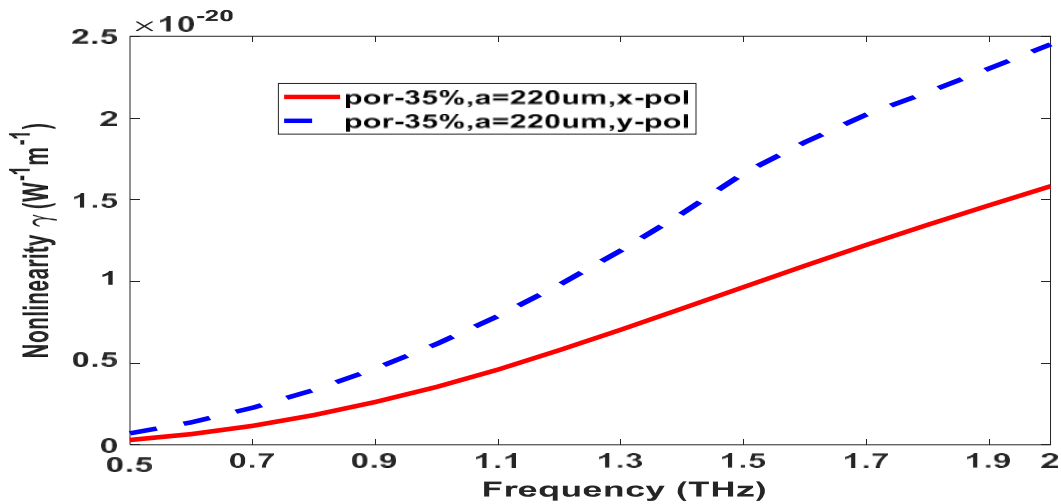


Figure 5.30: Non-linearity of the fiber as a function of frequency at  $2a=440\mu\text{m}$  for model 2

Table 5.1 shows a comparison of different characteristics of our proposed waveguide with some other porous core waveguides.

Ref.	Bulk Material	$f$ (THz)	B	$\pm\Delta\beta_2$ (ps/THz/cm)	$\alpha_{eff}$ (cm <sup>-1</sup> )	$L_{con}$ (cm <sup>-1</sup> )	Core Power Fraction (%)
[54]	TOPAS	0.85	0.033	-	0.099	10 <sup>-3.8</sup>	32.5
[55]	TOPAS	1	0.0483	$\pm 0.51$	0.085	4.39 $\times 10^{-4}$	37
[37]	TOPAS	1	0.045	$\pm 0.26$	0.08	-	33
[56]	TOPAS	0.7	0.01	$\pm 0.55$	0.07	-	-
[21]	TOPAS	1	0.00123	$\pm 0.09$	0.034	10 <sup>-3.7</sup>	44
[57]	TOPAS	1	0.086	$\pm 0.07$	0.05	10 <sup>-9</sup>	-
[19]	Zeonex	1.1	0.063	$\pm 0.02$	0.06	3.6 $\times 10^{-2}$	44
[17]	Zeonex	1	0.079	$\pm 0.05$	0.05	7.24 $\times 10^{-7}$	44
Proposed Model 1	Zeonex	1	0.0818	$\pm 0.08$	0.044	4 $\times 10^{-7}$	55.3
Proposed Model 2	Zeonex	1	0.1116	$\pm 0.45$	0.04716	2.65 $\times 10^{-7}$	35

Table 5.1: Comparison of different characteristics of the proposed PCFs with some other PCF's.

## 5.4 Fabrication Possibilities

The most important issue in designing a porous core fiber is its practical implementation. There are several fabrication methods[41,58,59] proposed by different researchers. The most commonly developed methods are capillary stacking, drilling, stack and draw, extrusion[60,61] and sol-gel etc. Among them, capillary stacking, stack and drilling and sol-gel techniques are only used to fabricate circular air holes. Several PCFs with different lattice structures have been fabricated by the Max Plank Institute. Extrusion technology can be used to fabricate almost all types of structures proposed by H. Ebendorff-Heidepriem et al. and Kiang et al.. Slotted structured air-holes using extrusion technique has also been fabricated by Atakaramians et al.. Moreover, Liu et al. fabricated elliptical air-holes by

methyl methacrylate (MMA) monomer polymerization method. In addition, micro-structured polymer optical fiber with asymmetric air-holes can be fabricated using 3D printing technology[62]. After analyzing the existing fabrication techniques, it can be concluded that our proposed model consisting of circular and non-circular air holes is practicable using extrusion technique.

## **5.5 Conclusion**

The results from our thesis are presented in this chapter. Effective material loss, birefringence and dispersion curves are shown in purpose. We have come to the decision that both of our proposed models show fairly good results. In the comparison table 5.1, although birefringence for model 2 is higher than that of model 1, we select model 1 because of lower material loss, lower dispersion and higher power fraction. According to our modeling, we can fabricate a waveguide which can play a vital role in THz communication and sensing applications.

# Chapter 6

## CONCLUSION

### 6.1 Introduction

In case of THz fiber, we see that, different application requires different parameters to change. If we want to use the fiber for communication purpose, we have to put effort on lowering absorption loss and dispersion. Moreover, if we want to use fiber for sensing purpose, we have to be aware about having higher birefringence.

We have plotted simulated results for various losses, dispersion, birefringence and non-linearity against various frequency and core length. We have also compared them in a table with previously proposed models. The table shows favorable results compared to other previously proposed models.

### 6.2 Conclusion

In this work, we present two numerical models of single mode novel porous core fiber. One has a core consisting of both circular and elliptical shaped air holes surrounded by cladding of slotted air-holes and another has an elliptical shaped suspended core. Numerical analysis of model 1 at optimum design parameters shows an ultra high birefringence of 0.0818, lower absorption loss of only  $0.0448 \text{ cm}^{-1}$ , a negligible confinement loss of  $4 \times 10^{-7} \text{ cm}^{-1}$  and a very low dispersion with flattened characteristics of  $1.162 \pm 0.05 \text{ ps/THz/cm}$  over a wide terahertz band. Furthermore, the proposed model 1 displays an extremely higher core power fraction of 55.3% and a negligible nonlinearity of  $3.33 \times 10^{-9} \text{ W}^{-1} \text{ m}^{-1}$  due to higher effective area.

On the other hand, Numerical analysis of the model 2 at optimum design parameters shows an ultra high birefringence of 0.1116 which is the highest so far to the best of our knowledge, lower absorption loss of  $0.04716 \text{ cm}^{-1}$ , a negligible confinement loss of  $2.65 \times 10^{-7} \text{ cm}^{-1}$  and a low flat dispersion flattened characteristics over a wide terahertz band. Furthermore, the proposed model 2 allows a significant amount of total power to flow through the core air-

slots. Moreover, due to its larger effective area, the proposed PCF demonstrates negligible non-linearity.

Both of the proposed model can be fabricated by extrusion technique. Considering their excellent modal characteristics, it is expected that the proposed model 1 can be used satisfactorily in long distance multichannel communication in THz band as well as in different polarization preserving applications while model 2 can be used only in polarization preserving applications.

### **6.3 Future Work**

In our thesis work, we tried to improve some particular properties keeping others in a tolerable range. Hence, there is scope of improving other properties. Besides, we could not fabricate the proposed fiber which is also a big challenge. Moreover, there are also some nonlinear properties which have great impact. We could not find these effects because of constraints of time and resource. Those properties should also be taken under consideration while designing a THz fiber.

However, we do believe that our model will have an impact on showing the way to design better THz fibers. We hope, our attempt of using Zeonex as a base material will have a contribution of introducing effective THz waveguides with most favorable characteristics.



## References

- [1] Fitch, M. J., and Osiander, R., "Terahertz waves for communications and sensing," *Johns Hopkins APL Tech. Dig.*, vol. 25, pp. 348–355, 2004.
- [2] Humphreys, K., Loughran, J.P., Gradziel, M., Lanigan, W., Ward, T., Murphy, J.A., and O'Sullivan, C., "Medical applications of terahertz imaging: a review of current technology and potential applications in biomedical engineering," in *IEEE conference of Eng Med Biol*, vol. 2, pp. 1302–1305 (2014).
- [3] Withayachumnankul, W., Png, G.M., Yin, X., Atakaramians, S., Jones, I., Lin, H., Ung, S.Y., Balakrishnan, J., Ng, B.W.H., Ferguson, B., Mickan, S.P., Fischer, B.M., and Abbott, D., "T-ray sensing and imaging," *Proc. of the IEEE*, vol. 95, pp. 1528–1558 (2007).
- [4] Withayachumnankul, W., *Engineering Aspects of Terahertz Time-Domain Spectroscopy*, 404 (2009).
- [5] Kulesa, C., "Terahertz spectroscopy for astronomy: From comets to cosmology," *IEEE Trans. Terahertz Sci. Technol.*, vol. 1, pp. 232–240, 2011.
- [6] Akyildiz, I. F., Jornet, J. M., and Han, C., "Terahertz band: Next frontier for wireless communications," *Phys. Commun.*, vol. 12, pp. 16–32, 2014.
- [7] Yetimoglu NO, K.K., "Applications of Terahertz Imaging in Medicine," *Omi. J. Radiol.*, vol. 03, p. 7964, 2014.
- [8] Pickwell, E., Wallace, V.P., "Biomedical applications of terahertz technology," *J. Phys. D. Appl. Phys.*, vol. 39, pp. 301–310, 2006.
- [9] Cunin, F., Schmedake, T.A., Link, J.R., Li, Y.Y., Kom, J., Bhatia, S.N., and Sailor, M.J., "Biomolecular screening with encoded porous-silicon photonic crystals," *Nat. Mater.*, vol. 1, pp. 39–41, 2002.
- [10] Morshed, M., Asaduzzaman, S., Arif, M.F.H., and Ahmed, K., "Proposal of simple gas sensor based on micro structure optical fiber," in *2015 Int. Conf. Electr. Eng. Inf. Commun. Technol.*, vol. 2, pp. 1–5 (2015).

- [11] Han, H., Park, H., Cho, M., and Kim, J., "Terahertz pulse propagation in a plastic photonic crystal fiber," *Appl. Phys. Lett.*, vol. 80, pp. 2634–2636, 2002.
- [12] Goto, M., Quema, A., Takahashi, H., Ono, S., and Sarukura, N., "Teflon Photonic Crystal Fiber as Terahertz Waveguide," *Japanese J. Appl. Phys.*, vol. 43, pp. 2–5, 2004.
- [13] Nielsen, K., Rasmussen, H.K., Adam, A.J., Planken, P.C., Bang, O., and Jepsen, P.U., "Bendable, low-loss Topas fibers for the terahertz frequency range," *Opt. Express.*, vol. 17, p. 8592, 2009.
- [14] Yuan, W., Khan, L., Webb, D.J., Kalli, K., Rasmussen, H.K., Stefani, A., and Bang, O., "Humidity insensitive TOPAS polymer fiber Bragg grating sensor," *Opt. Express.*, vol. 19, p. 19731, 2011.
- [15] Islam, M.S., Sultana, J., Rana, S., Islam, M.R., Faisal, M., Kaijage, S.F., and Abbott D., "Extremely low material loss and dispersion flattened TOPAS based circular porous fiber for long distance terahertz wave transmission," *Opt. Fiber Technol.*, vol. 34, pp. 6–11, 2017.
- [16] Emiliyanov, G., Jensen, J.B., Bang, O., Hoiby, P.E., Pedersen, L.H., Kjaer, E.M., and Lindvold, L., "Localized biosensing with Topas microstructured polymer optical fiber," *Opt. Lett.*, vol. 32, pp. 460–462, 2007.
- [17] Islam, M.S., Sultana, J., Dinovitser, A., Ng, B.W.H., and Abbott, D., "A novel Zeonex based oligoporous-core photonic crystal fiber for polarization preserving terahertz applications," *Opt. Commun.*, vol. 413, pp. 242–248, 2018.
- [18] Woyessa, G., Fasano, A., Markos, C., Stefani, A., Rasmussen, H.K., and Bang, O., "Zeonex microstructured polymer optical fiber: fabrication friendly fibers for high temperature and humidity insensitive Bragg grating sensing," *Opt. Mater. Express.*, vol. 7, p. 286, 2017.
- [19] Islam, M.S., Sultana, J., Dinovitser, A., Faisal, M., Islam, M.R., Ng, B.W.-H., and Abbott, D., "Zeonex-based asymmetrical terahertz photonic crystal fiber for multichannel communication and polarization maintaining applications," *Appl. Opt.*, vol. 57, p. 666, 2018.

- [20] <https://www.zeonex.com> (accessed at 22:10 p.m. on 06-06-2018).
- [21] Islam, M.S., Sultana, J., Atai, J., Islam, M.R., and Abbott, D., "Design and characterization of a low-loss, dispersion-flattened photonic crystal fiber for terahertz wave propagation," *Optik (Stuttg)*, vol. 145, pp. 398–406, 2017.
- [22] Zhan, H., Mendis, R., and Mittleman, D.M., "Characterization of the terahertz near-field output of parallel-plate waveguides," *J. Opt. Soc. Am. B.*, vol. 28, pp. 558–566, 2011.
- [23] Bowden, B., Harrington, J.A., and Mitrofanov, O., "Low-loss modes in hollow metallic terahertz waveguides with dielectric coatings," *Appl. Phys. Lett.*, vol. 93, pp. 2008–2010, 2008.
- [24] Wang, D.M., and Mittleman, K., "Metal wires for terahertz waveguiding," *Nature*, vol. 432, pp. 376–379, 2004.
- [25] Doradla, P., Joseph, C.S., Kumar, J., and Giles, R.H., "Propagation loss optimization in metal/dielectric coated hollow flexible terahertz waveguides," vol. 8261, p. 82610P, 2012.
- [26] Russell, P.S.J., Hölzer, P., Chang, W., Abdolvand, A., and Travers, J.C., "Hollow-core photonic crystal fibres for gas-based nonlinear optics," *Nat. Photonics.*, vol. 8, pp. 278–286, 2014.
- [27] Bledt, C.M., and Harrington, J. a., "Silver and silver / polystyrene coated hollow glass waveguides for the transmission of visible and infrared radiation," *Proc. SPIE.*, vol. 8218, pp. 821809–821810, 2012.
- [28] Bowden, B., Harrington, J.A., and Mitrofanov, O., "Silver/polystyrene coated hollow glass waveguides for the transmission of THz radiation," in *Conference on Lasers and Electro-Optics*, vol. 32, pp. 2945–2947 (2007).
- [29] Pristiniski, D., and Du, H., "Solid-core photonic crystal fiber as a Raman spectroscopy platform with a silica core as an internal reference," *Opt. Lett.*, vol. 31, pp. 3246–3248, 2006.
- [30] Atakaramians, S., V., S.A., Ebendorff-Heidepriem, H., Nagel, M., Fischer, B.M.,

- Abbott, D., and Monro, T.M., "THz porous fibers: design, fabrication and experimental characterization," *Opt. Express.*, vol. 17, pp. 14053–14062, 2009.
- [31] Islam, M.S., Rana, S., Islam, M.R., Faisal, M., Rahman, H., and Sultana, J., "Porous core photonic crystal fibre for ultra-low material loss in THz regime," *IET Commun.*, vol. 10, pp. 2179–2183, 2016.
- [32] Aljunid, S., Ahmad, B., Ali, S., and Ahmed, N., "Ultra-flat low material loss porous core THz waveguide with near zero flat dispersion," *Electron. Lett.*, vol. 52, pp. 863–865, 2016.
- [33] Islam, R., and Rana, S., "Dispersion flattened , low-loss porous fiber for single-mode terahertz wave guidance," *Opt. Eng.*, vol. 54, p. 055102, 2015.
- [34] Islam, M.S., Sultana, J., Atai, J., Abbott, D., Rana, S., and Islam, M.R., "Ultra low-loss hybrid core porous fiber for broadband applications," *Appl. Opt.*, vol. 56, p. 1232, 2017.
- [35] Chen, N., Liang, J., and Ren, L., "High-birefringence, low-loss porous fiber for single-mode terahertz-wave guidance," *Appl. Opt.*, vol. 52, pp. 5297–5302, 2013.
- [36] Hasan, M.R., Islam, M.A., and Rifat, A.A., "A single mode porous-core square lattice photonic crystal fiber for THz wave propagation," *J. Eur. Opt. Soc.*, vol. 12, pp. 1-8, 2016.
- [37] Islam, R., Habib, M. S., Hasanuzzaman, G.K.M., Rana, S., and Sadath, M. A., "Novel porous fiber based on dual-asymmetry for low-loss polarization maintaining THz wave guidance," *Opt. Lett.*, vol. 41, p. 440, 2016.
- [38] Wang, C., Zhang, J., Zhang, C., He, J., Lin, Y., Jin, W., Liao, C., Wang Y., and Wang, Y., "Bragg Gratings in Suspended-Core Photonic Microcells for High-Temperature Applications," *J. Light. Technol.*, vol. 36, pp. 2920–2924, 2018.
- [39] Dauliat, R., Gaponov, D., Benoit, A., Salin, F., Schuster, K., Jamier, R., and Roy, P., "Inner cladding microstructuration based on symmetry reduction for improvement of singlemode robustness in VLMA fiber," *Opt. Express.*, vol. 21, p. 18927, 2013.

- [40] Ponseca, C.S., Jr., Pobre, R., Estacio, E., Sarukura, N., Argyros, A., Large, M.C., and van Eijkelenborg, M., "Transmission of terahertz radiation using a microstructured polymer optical fiber," *Opt. Lett.*, vol. 33, p. 902, 2008.
- [41] Issa, N.A., van Eijkelenborg, M.A., Fellew, M., Cox, F., Henry, G., and Large, M.C.J., "Fabrication and study of microstructured optical fibers with elliptical holes," *Opt. Lett.*, vol. 29, pp. 1336–1338, 2004.
- [42] [https://www.rp-photonics.com/terahertz\\_radiation.html](https://www.rp-photonics.com/terahertz_radiation.html) (accessed January 1, 2019).
- [43] <https://www.azom.com/article.aspx?ArticleID=788> (accessed November 26, 2018).
- [44] <http://www.upcinc.com/resources/materials/HDPE.html> (accessed January 2, 2019).
- [45] <https://www.azom.com/article.aspx?ArticleID=423> (accessed December 13, 2018).
- [46] <http://textilelearner.blogspot.com/2013/04/teflon-ptfe-polytetrafluoroethylene.html> (accessed December 15, 2018).
- [47] <https://www.comsol.com/multiphysics/finite-element-method> (accessed December 20, 2018).
- [48] Rana, S., Islam, M. S., Faisal, M., Roy, K.C., Islam, R., and Kaijage, S.F., "Single-mode porous fiber for low-loss polarization maintaining terahertz transmission," *Opt. Eng.*, vol. 55, p. 076114, 2016.
- [49] Islam, S., Islam, M.R., Faisal, M., Arefin, A.S.M.S., Rahman, H., Sultana, J., and Rana, S., "Extremely low-loss, dispersion flattened porous-core photonic crystal fiber for terahertz regime," *Opt. Eng.*, vol. 55, p. 076117, 2016.
- [50] Mia, M.B., Ani, A.B., Chowdhury, K.R., and Faisal, M., "Highly nonlinear and low confinement loss photonic crystal fiber using GaP slot core," in *2nd IEEE Int. Conf. Telecommun. Photonics*, vol. 2017–Decem, pp. 10–13 (2018).
- [51] Rana, S., Rakin, A.S., Hasan, M.R., Reza, M.S., Leonhardt, R., Abbott, D., and Subbaraman, H., "Low loss and flat dispersion Kagome photonic crystal fiber in the terahertz regime," *Opt. Commun.*, vol. 410, pp. 452–456, 2018.
- [52] Chen, D., and Tam, H.Y., "Highly birefringent terahertz fibers based on super-cell

- structure," *J. Light. Technol.*, vol. 28, pp. 1858–1863, 2010.
- [53] Singh, S.P., and Singh, N., "Nonlinear Effects in Optical Fibers: Origin, Management and Applications," *Prog. Electromagn. Res. PIER.*, vol. 73, pp. 249–275, 2007.
- [54] Wu, Z., Shi, Z., Xia, H., Zhou, X., Deng, Q., Huang, J., Jiang, X., and Wu, W., "Design of highly birefringent and low-loss oligoporous-core thz photonic crystal fiber with single circular air-hole unit," *IEEE Photonics J.*, vol. 8, pp. 2–10, 2016.
- [55] Hasan, M. R., Anower, M. S., Islam, M. A., and Razzak, S.M.A., "Polarization-maintaining low-loss porous-core spiral photonic crystal fiber for terahertz wave guidance," *Appl. Opt.*, vol. 55, p. 4145, 2016.
- [56] Islam, R., Habib, M.S., Hasanuzzaman, G.K.M., Rana, S., Sadath, M.A., and Markos, C., "A Novel Low-Loss Diamond-Core Porous Fiber for Polarization Maintaining Terahertz Transmission," *IEEE Photonics Technol. Lett.*, vol. 28, pp. 1537–1540, 2016.
- [57] Sultana, J., Islam, M.S., Faisal, M., Islam, M.R., Ng, B.W.H., Ebendorff-Heidepriem, H., and Abbott, D., "Highly birefringent elliptical core photonic crystal fiber for terahertz application," *Opt. Commun.*, vol. 407, pp. 92–96, 2018.
- [58] <https://www.mpl.mpg.de/en/russel/research/topics/fabrication.html> (accessed January 1, 2019).
- [59] Vaca-Pereira, M., Minkovich, V.P., and Calixto, S., "Fabrication and investigation of large-mode-area photonic crystal fibers," *Rev. Mex. Fis.*, vol. 59, pp. 317–321, 2013.
- [60] Ebendorff-Heidepriem, H., and Monro, T.M., "Extrusion of complex preforms for microstructured optical fibers," *Opt. Express.*, vol. 15, pp. 15086–15092, 2007.
- [61] Kiang, K.M., Frampton, K., Monro, T.M., Moore, R., Tucknott, J., Hewak, D.W., Richardson, D.J., and Rutt, H.N., "Extruded singlemode non-silica glass holey optical fibres," *Electron. Lett.*, vol. 38, p. 546, 2002.
- [62] Ebendorff-Heidepriem, H., Schuppich, J., Dowler, A., Lima-Marques, L., and Monro, T.M., "3D-printed extrusion dies: a versatile approach to optical material processing," *Opt. Mater. Express.*, vol. 4, p. 1494, 2014.

- [63] Mishra, S., and Singh, V., "Investigation of phase birefringence and group birefringence of square size photonic crystal fiber at wavelength 1.3  $\mu\text{m}$ ," *Optik*, vol. 124, pp. 1294-1296, 2013.
- [64] Bao, H., Nielsen, K., Rasmussen, H. K., Jepsen, P. U., and Bang, O., "Fabrication and characterization of porous-core honeycomb bandgap THz fibers, " vol. 20, pp. 3457–3459, 2012.